Scientific Research Publishing

International Journal of Clinical Medicine, 2024, 15, 299-334
https://www.scirp.org/journal/ijcm
ISSN Online: 2158-2882
ISSN Print: 2158-284X

Preclinical Verification of Modulated Electro-Hyperthermia

—Part II. *In Vivo* Research

Andras Szasz

Department of Biotechnics, Hungarian University of Agriculture and Life Sciences, Gödöllő, Hungary
Email: szasz.andras@gek.szie.hu

How to cite this paper: Szasz, A. (2024) Preclinical Verification of Modulated Electro-Hyperthermia—Part II. *In Vivo* Research. *International Journal of Clinical Medicine*, **15**, 299-334.
https://doi.org/10.4236/ijcm.2024.157020

Received: June 19, 2024
Accepted: July 28, 2024
Published: July 31, 2024

Abstract

The treatments of malignant diseases nowadays are rapidly developing. One of the groups of novel therapies applies electromagnetic fields to destroy the malignant lesions. The thermal (heating) and nonthermal (polarization, molecular excitations) processes are combined in novel methods. The non-ionizing energy absorption from the electric field may produce substantial heat, increasing the targeted lesion's temperature and inducing hyperthermic effects. The modulated electro-hyperthermia (mEHT) uses thermal conditions to optimize and accelerate the chemical reactions induced by the nonthermal excitation of the electric field. The mEHT cooperates with the body's homeostatic control and harmonizes the mutual efforts to destroy the malignancy. Our objective is to show *in vivo* proof of the combined complementary electromagnetic impact on various tumors produced by mEHT. Furthermore, we present evidence of the increasing efficacy of the complementary application of mEHT with conventional treatments.

Keywords

mEHT, Cancer Treatment, Thermal, Nonthermal, Electric, *In Vivo*, Tumor Destruction

1. Introduction

Cancer therapies have rapidly developed in the last decades [1]. All classical treatments like chemotherapy (ChT), radiotherapy (RT), and surgery (Op) went through intense development. The new highly effective pharma products, the personalized and targeted approaches, the complex, versatile protocols, and the precise pointing of malignant lesions increased the success rate of the conventional treatment.

New therapies focus on extending patient survival with an acceptable quality of life. Despite the robust development, the estimated 2+ million new cases in 2024 [2] derail the optimistic and encouraging outlook for cancer care. Intensive efforts in drug development drive the progress of cancer therapies. Another challenge, however, is the present oncotherapies have severe adverse effects and toxicity, which limits their applications. There are 95% of the new cancer drugs applied in clinical studies have no approval because of their high toxicity [3]. Nonionizing electromagnetic therapies group different approaches without chemical toxicity. Like radiotherapy (ionizing radiation), electromagnetic energy absorption could cause thermal toxicity (burns), which differs from other adverse effects. This toxicity does not develop comorbidities. Avoiding its side effects or treating the accidentally appearing one is relatively easy. The electromagnetic impact on chosen reactions could increase the efficacy and decrease the toxicity of the complementary applied therapy [4]-[6]. The selection of malignancy by biophysical effects looks optional [7] [8], and the thermal effects of the nonionizing could accelerate the excited chemical reactions (but chemically active) electromagnetic radiation [9]. These advantages support electromagnetic energy absorption as a helpful therapy, both standalone and in complementary applications.

The chemically active nonthermal electromagnetic effects are calculated and verified *in vitro* cell culture experiments [10]. The synergy of thermal and nonthermal effects had been measured *in vitro* but the selectivity considering intensive physiological feedback can be studied only *in vivo*. The present part of the series aims to show the *in vivo* research and review its results.

2. Method

The modulated electro-hyperthermia (mEHT) technical solution is classical capacitive coupling with radiofrequency (RF) application at 13.56 MHz. A plan-parallel condenser provides the energy to the experimental animal between the electrodes, which are asymmetric [11].

The mEHT is a hyperthermia method, which, in addition to the thermal energy absorption, uses nonthermal, electric field-dependent molecular excitations, increasing the tumor-destruction facility of the energy [7]. mEHT targets the electric and thermal differences between the malignant and healthy tissues and the micro heterogeneities at the tumor microenvironment (TME) [9]. The electric field selects the highly proliferative tumors by their high electric conductivity, and the low-frequency amplitude modulation active in polarization and molecular excitations of transmembrane proteins of the malignant cells [5] [6]. Various apoptotic signals are excited by external electric field impact. The frequencies are optimized fro the best performance [5] [8]. The electric field selects the tumor, and the low-frequency amplitude modulation polarizes and excites the transmembrane proteins of the malignant cells. The primary guidance of mEHT is biophysical using updated bioelectromagnetic considerations. The selective targeting modifies the conventional hyperthermia which intends to heat the entire mass of the tuor iso-

thermally. The heterogeneous heating uses the thermal effects on the targeted molecules to accelerate the signal transduction which is triggered by the nonthermal impact [12]. The transmembrane molecular targeting of nonionizing radiation by a modulated electric field is like the ionizing radiation (radiotherapy, RT), which targets also molecular components in the strand of DNA.

The devices for *in vivo* use were the LabEHT100 and LabEHY200 (Oncotherm, Budaors, Hungary). The animal lies on the rectangular-shaped 6 × 12 cm size grounded electrode. To prevent the mice from cooling, the temperature of the counter electrode was controlled; it was kept at 37˚C during the treatment. The round-shaped opposing electrode (applicator) is above the animal, is 18 mm in size, and can be adjusted with a flexible holder to the necessary position above the treated tumor. A bolus with distilled water ensures optimal electromagnetic coupling. The applicator is cooled with circulating water. The allometric scaling estimates the speed of mice physiology (including the heartbeats) to be seven times quicker than that of humans. Due to the rapid physiological feedback, an ultrafast tuning system makes the prompt automatic adjustment of animal reactions possible. The temperature intratumoral, skin, and rectal measured, and the electric tuning status with the forwarded and reflected powers are also registered in real-time. The sampling frequency is 60/min. The temperature was controlled with specialized thermometers immune to RF radiation. The experimental conditions are discussed in detail in every referred article.

The animals are anesthetized during the treatment. The experimental setup is shown in Figure 1.

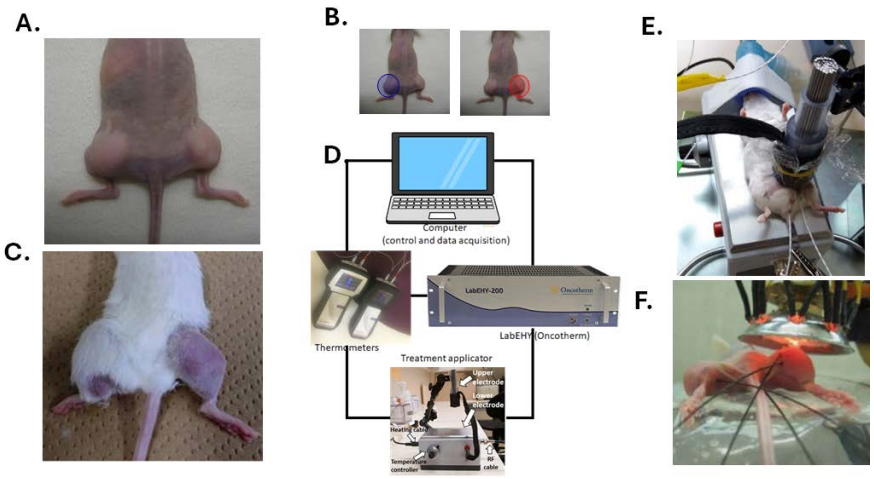

Figure 1. Experimental setup of the *in vivo* experiments. Some experimental animals had their own untreated control tumor in a symmetrical position, usually in the left and right femoral regions. (A.) In the immunocompromised (nude) mice, the two tumors are supposed to be independent. (B.) Only one tumor is treated (always the right side) with mEHT; the other is used for comparison. In immunocompromised nude mice, the untreated tumor is regarded as a control. (C.) In immunocompetent mice, we expect immune reactions. The two tumors distantly inoculated tumors are connected, making it possible to measure the abscopal effect in distant locations. (D.) The measuring setup. (E.) mEHT treatment of a mouse. (F.) Infrared hyperthermia (iHT) treatment.

Numerous cancer-bearing companion animals (dogs and cats) were successfully treated with mEHT [13]. These treatments better approach human tumorous cases because they have larger body weights than rodents. The larger body mass shifts the physiological timing to longer scales, better approaching human conditions. The naturally developed, not inoculated tumors also allow these treatments to be closer to human studies.

The technical details of the treatment are described elsewhere [14]-[17]. The treatment conditions mostly follow a standard protocol of 42˚C in the tumor for 30 min. The time from the inoculation of the tumor cells to the first mEHT treatment depends on the tumor size, which is approximately 2 g when the experimental process starts. In some experiments, Matrigel is used to control growth. The applied power varies by the animals and their tumors, ranging from 1 W to 8 W. The treated tumors were studied using various methods. The tumor in its 3D form was studied with size (caliper and ultrasound) and its activity (bioluminescence signals). The excised *ex vivo* tumors were characterized by their size/weight. The tumors are usually cut in half; one is frozen, formalin-fixed, and embedded in paraffin for further investigation. The frozen samples are helpful for genetic and protein analysis and Western blot, FACS, PCR, the paraffin-embedded samples for morphological studies, multiple immunohistochemistry, and signal pathway analyses; the most frequent processes with then excised samples are shown in Figure 2.

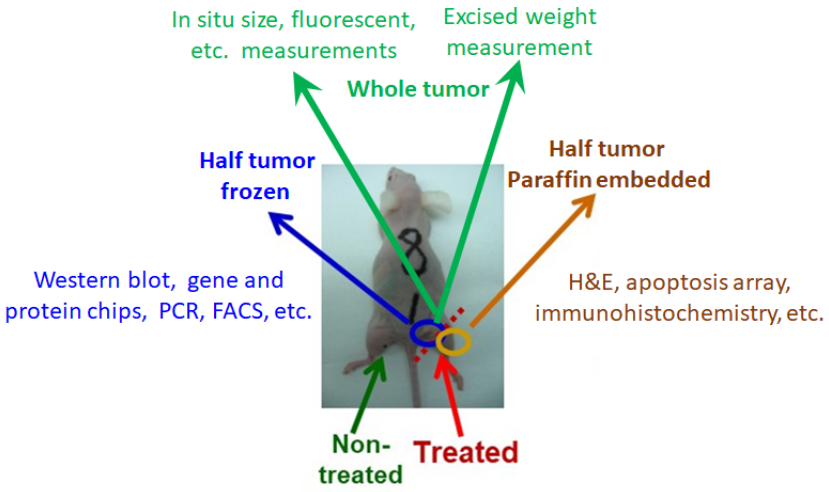

Figure 2. In immunocompromised mice, the primary measurement categories of the treated tumor are as follows: the whole tumor is measured in situ, while the excised (*ex vivo*) tumors, after measuring their weight, are halved, serving different measurements.

The results are compared to sham mEHT treatment, infrared hyperthermia, or distant, untreated tumors in the same animal.

3. *In Vivo* Measurements

The publications on *in vivo* measurements are collected in Table 1.

Table 1. *In vivo* preclinical research.

Tumor cells	Method	Result	Conclusion	Ref.
FSaII was inoculated into the femoral region of the C3H mice and treated with mEHT and RT.	mEHT 41˚C, 10 + 30 min, 2 - 3 W, plus irradiation 15 Gy (1.3 Gy/min). Studied the tumor growth, apoptosis, and HIF-1*a*, VEGF, and CA-9 were measured.	The tumor growth was inhibited, and the apoptosis rate increased with the combined treatment. Furthermore, it reduced the RT, increased hypoxia, and increased blood perfusion.	The combined treatment enhances the anti-tumor effect of high-dose irradiation and minimizes the side effects of the RT.	[18]
RG2 [D74] glioma cell line was inoculated into the parietal lobe of syngeneic Fischer 344 rats, treated with pulsed mEHT.	MRI was measured on the 8th and 15th days after inoculations. Four groups of animals were compared using sham, mEHT stand-alone, mEHT + TMZ, and the pulsed mEHT in a time-course protocol.	The pulsed mEHT was superior to all other treatment groups.	The pulsed mEHT looks like a further novel development of the conventional mEHT method.	[19]
4T1 was inoculated into BALB/c mice, isograft, and treated with mEHT.	mEHT 42˚C, 5 + 30 min, (skin 39.5˚C, body 37.8˚C.) Apoptosis was measured with multiple other characteristics of change in time course.	HSP70 was significantly induced by mEHT, with a maximum of 12 h after treatment. The cell destruction and cC3 have their maximum at 24 h, and the viability is significantly decreased. 5 mEHT treatment significantly suppressed the Ki67 proliferation marker.	The massive HSP70 development exhausts the cells and plays a major role in losing cell protection against stress, consequently promoting cellular destruction.	[20]
Huh-7 and HepG2 cell lines xenograft in nude mice treated with mEHT.	mEHT 42˚C, 5 + 30 min, (skin 39.5˚C, body 37.8˚C) caliper ruler monitored.	mEHT significantly inhibited the growth of human HCC xenografts in nude mice.	On the 19th day, the control tumor was double that of the mEHT-treated one.	[21]
U87-MG and A172 human glioma cells inoculated into BALB/c nude mice xenograft.	mEHT 42˚C, 30 min, 3 W (3x), time course study. RNA sequencing a caliper ruler was used.	Inhibited tumor growth, significant apoptotic rate, reduced cell migration.	Increased p53 and E2F1, reduced PARP1 in mRNA level, suppressed CD133+ cancer stem cells.	[22]
HT29 human metastatic colorectal xenograft model. BALB/c nude mice.	mEHT 42˚C, 30 min, 4 W, time-course study with Immunohistochemistry, Western blot, TUNEL assay.	Significant apoptosis of the malignant cells, DNA fragmentation, AIF mediated apoptotic pathway.	Caspase-independent apoptosis, with mitochondrial permeabilization and DNA fragmentation.	[23]

Continued

HT29 xenograft model, BALB/c nude mice treated with mEHT.	mEHT 42˚C, 30 min, 4 W, time-course study with Immuno-histochemistry, microarray, apoptosis array,	Measured damage-associated molecular pattern (HSP70, CRT, HMGB1 and HSP90).	mEHT induces a spatiotemporal sequence of DAMP signals HT29 cancer, and it can be a potential local inducer of immunogenic cell death.	[24]
HT29 xenograft model. MEHT treated BALB/c nude mice.	mEHT 42˚C, 30 min, 4 W, time-course study with Immunohistochemistry, apoptosis analysis.	mEHT caused selective tumor destruction, and upregulation of TRAIL-R2 and FAS was observed.	mEHT caused massive caspase-independent cell death.	[25]
C26 allografts of immunocompetent (BALB/c) mice plus immunostimulant MTE.	mEHT 42˚C, 30 min, 1 - 3 W, Immunohistochemistry, TUNEL assay apoptosis analysis, comparison of the treated and nontreated tumors of the same mouse. Extra immune stimulant (MTE) is applied.	The damage-associated molecular pattern was measured (CRT, HSP70, HMGB1). Ki67 was suppressed. Dendritic cells were matured, and antigen-presenting showed tumor-specific killer T-cells and their invasion into the tumor.	The mice with immune stimulants had an abscopal effect, showing the same development in the untreated tumor as in the treated one. ICD formed tumor-specific immune reactions.	[26]
CT26 allografts of immunocompetent (BALB/c) mice plus dendritic cell immunostimulant.	mEHT 42˚C, 30 min, DC cells inoculated intratumorally to the femoral area, cytotoxic T lymphocyte assay, ELISPOT, Immunohistochemistry.	Significant HSP70 release was measured in comparison to wHT with the same temperature. The DC-combined mEHT inhibited cell growth, and the substantial appearance in CD45+, F4/80, and Eosinophil leukocytes were measured.	mEHT can create a favorable tumor microenvironment for an immunological chain reaction. Rechallenging the same tumor was ineffective. The DC-combined mEHT worked as an antitumor-vaccination.	[27]
A2058 human melanoma cell line and NK cell immunotherapy combined with mEHT.	mEHT 42˚C, 30 min, NK cells or IL-2 independent NK-92MI injected subcutaneously to right and left femoral region. Only the right side was treated.	Intensive hsp70 expression followed by significant upregulation of cC3 and p53. NK cell accumulation was in the treated tumor but not in the untreated side. Upregulation of CXCL11 and MMP2 was observed.	mEHT ultimately leads to completely eradicating melanoma and appears to be a good combination with NK immunotherapy.	[28]
CT26/BALB/c mice tumor model mEHT with Cur and Res combined treatment.	mEHT 42˚C, 30 min, 10 - 12 W, tumor growth, and immune cell infiltration were measured together with cell viability, apoptosis, Western blot, and immunohistochemistry comparison with wHT.	mEHT with Cur and Res combination inhibited the growth of CT26 cancer by inducing apoptosis and HSP70 expression of tumor cells while recruiting CD3+ T-cells and F4/80+ macrophages.	Cur and Res combined with mEHT synergistically increased HSP release and immune response, showing enhanced anti-tumor efficacy.	[29]

Continued

B16F10 allograft cells inoculated to female C57Bl/6 mice (offspring of C57Bl/6 colonies) in the right inguinal area.	mEHT 42˚C, 30 min, measured tumor-size, HSP70, PUMA, γH2AX, DAMP signaling was measured.	Upregulation of cytoplasmic and cell membrane HSP70 Increased PUMA and AIF1 and rise of cC3 without significant apoptosis. But, γH2AX indicated DNA double-strand breaks, which upregulated p53 protein and downstream p21waf1 and p27kip. mEHT promoted the release of DAMP; it reduced MHC-I levels in tumor cells.	mEHT-related tumor shrinkage was primarily mediated by p53, upregulating the cyclin-dependent kinase inhibitors. Reduced cytotoxic T-cell response was observed despite increased DAMP signaling. Decreased tumor antigen and MHC-I levels suggest that NK cells and macrophages were the major contributors to tumor eradication.	[30]
FSaIIcells inoculated subcutaneously in the femoral region of C3H mice. mEHT plus 15 Gy RT, with Mef, was applied.	mEHT 41˚C, 30 min, metformin was intraperitoneal, 150 mg/kg. HIF-1α, VEGF, PD-L1, and TUNEL apoptosis were measured.	Irradiation markedly increased the expression of HIF-1 α, VEGF, PD-L1, and mEHT, which was reduced by the mEHT combined treatment and enhanced the suppression of tumor growth.	The increased tumor response to 15 Gy irradiation by mEHT and Mef alone or in combination was due, in part, to the abrogation of the radiation-induced upregulation of HIF-1α and its downstream targets VEGF and PD-L1.	[31]
A549 and NCI-H1299 cell-line BALB/c nude mice heterotopic xenograft treated with mEHT.	The linear-quadratic (LQ) model was used for an equivalent radiation dose of mEHT, 42˚C, 30 min.	mEHT + RT arrested the tumor growth, significantly increased the apoptosis.	The thermal enhancement of mEHT was determined, and the estimated equivalent radiation was calculated.	[32]
A549 and NCI-H1299 cell line BALB/c nude mice heterotopic xenograft treated with mEHT.	mEHT 42˚C, SAR = 250 W/kg, CEM43 dose calculated and compared to the measurements.	The tumor has > 3C higher temperature than the surrounding muscles, with good agreement with the numerical calculations. The tumor has > 4 times larger CEM43 than the surrounding.	The experiments proved the selection of the energy absorption, which is automatically well-localized on the tumor, and the host has less heating.	[33]
CT26 allografts of immunocompetent (BALB/c) mice plus liposomal Dox.	mEHT 42˚C, 30 min, tumor in femoral region, 10 mg/kg liposomal Dox. The effect was compared with wHT.	mEHT enhanced the liposomal Dox uptake. The combined treatment arrests the tumor growth. The effects were significantly higher than in wHT cases.	mEHT stimulated the activity of receptors and enzymes of cancer cells. Consequently, the uptake of Dox significantly increased after mEHT and effectively enhanced the drug's therapeutic effect.	[34]
The liver of a healthy pig was mEHT treated.	mEHT 150 W, 60 min, 540 kJ, anesthetized female pig 49.5 kg Immediate maximal, or step-up heating.	Shallow intrahepatic temperature > 42˚C, deep intrahepatic temperature > 41˚C, skin temperature < 41˚C, rectal temperature < 39˚C.	The measurements show a definite increase in the temperature of the liver of a living, anesthetized pig treated with mEHT.	[35]

Continued

Companion animals with mEHT are dedicated for veterinarian use.	VetEHY system treated dogs and cats. Step-up heating, < 35 W. Spontaneously occurring tumors.	All treated cases have shown remarkable improvement, tumor shrink, and better animal movability.	mEHT is a powerful veterinarian tool for companion animals and valuable for comparative clinical oncology.	[13]
mEHT was applied with a high Vitamin C dose for the C26 murine model.	Vit.C 2g/kg dose, mEHT 42˚C, 30 min.	A histopathological study was made *ex vivo* 24 hours after treatment. Vit.C had no effect as monotherapy. The combined treatment had high fluctuations. The tumor distribution was the same in both tumors of the animal.	The study does not allow a definite conclusion, but a sign of the possible abscopal effect was observed.	[36]
mEHT was used for the HT29 xenograft mouse model on female NMRI nu/nu mice.	mEHT 1 W, 5 + 30 min. < 40˚C, Bioluminescent method was used. Matching electric parameters were measured.	mEHT had significantly less dT/dt than EHT. However, the skin temperature and depth were slightly higher in mEHT. The matching impedances differ between the EHT and mEHT.	The study demonstrates the non-temperature-dependent anticancer effects of mEHT, shows the role of modulation, and promises more effective cancer therapy.	[37]
HT29 metastatic xenograft model. BALB/c nude mice treated with mEHT.	mEHT 42˚C, 30 min, 4 W, time-course study. TUNEL apoptosis analysis.	mEHT caused a selective tumor destruction, and upregulation of TRAIL-R2, FAS, FADD, SMACK/Diabolo, HTRA2/Omi HSP60 and HSP70 were measured.	mEHT treatment upregulates a range of proteins related to apoptosis induction and heat shock response within 24 hours post-treatment.	[38]
Human squamous cell lung cancer cell-line BALB/c nude mice heterotopic xenograft treated with mEHT.	mEHT 42˚C, 30 min, power < 2.5 W. Local temperature sensors: intratumoral, host tissue, rectal measurement. Conductivity and dielectric constant were also measured.	Tumor temperature 42˚C, muscle host 34˚C, rectum 30˚C, and the treatment bed 28˚C. The calculated simulation corresponds well with the measurements.	The measured temperature mapping and the thermal dose agree well with the numerical calculation.	[39]
mEHT for HT29 xenograft model. The irHT and mEHT at 42˚C, and mEHT at 38˚C, were compared.	mEHT and iHTwas 42˚C, 60 min (32 V/m field), and additional mEHT 38˚C. Micromorphological analysis 24 h after treatment.	The dead cell ratio was significantly higher with mEHT compared to other groups. Notably, the mEHT 38˚C, also did substantially better tumor destruction than the iHT on 42C.	A strong synergy of thermal and nonthermal components is shown, proving the importance of the nonthermal effects.	[40]
Effect of repeated mEHT treatment in 4T07 TNBC. 4T07 cells were inoculated orthotopically in female BALB/c mice.	mEHT 42˚C, 30 min, skin temperature just over the tumor 40˚C (3 W) The repeated treatments were studied by tumor size, cC3, HSP70, immune profile (CD3+, CTLA4, PD-1, PD-L1), p21, and Ki67.	The five-treatment repetition shows a significant positive change in all measured parameters in 4T07 TNBC.	Repeated treatment improves the effect of mEHT and is well applicable for TNBC tumors, suggesting positive clinical performance.	[41]

Continued

mEHT for B16F10 melanoma pulmonary metastases. Repeated treatment of lung.	mEHT 30 min, 42˚C (lung) 40˚C (pharyngeal) and 38.5˚C (rectal temperatures). Measured immunohistochemistry, flow cytometry, and apoptotic and necrotic cell death. 6 times repeated treatment.	mEHT induced significant anti-tumor effects and the downregulation of Ki67 expression, as well as made significant DNA double-strand breaks, significantly increased CD3+, CD8+ T-lymphocytes, and F4/80+CD11b+ macrophage density in the whole lung.	mEHT inhibits tumor growth and spontaneous proliferation of B16F10 melanoma in a mouse pulmonary metastasis model. mEHT is a complementary therapeutic option to chemo- and/or radiotherapy. The massive infiltration of tumors by CD3+ and CD8+ T-lymphocytes and by F4/80 CD11b-positive macrophages indicates the ability of mEHT to mobilize the immune response in treated animals.	[42]
mEHT for therapy-resistant TNBC model with 4T1 and 4T07 cell lines inoculated orthotopically into female BALB/c mice.	mEHT (5x) 42˚C, 30 min, skin temperature 40˚C. Measured properties: morphology, HSP70, Ki67, gene expression.	mEHT significantly inhibited tumor growth and diminished Ki67. It produced several stress-related factors. mEHT treatment induced innate immune-response reactions, among others, in the tumor. Thirteen stress-related genes were observed to be significantly upregulated.	mEHT has effective antitumor effects in the highly aggressive and rapidly growing 4T1/4T07 TNBC, even in monotherapy. The exhaustion of protective mechanisms diminished cancer proliferation and active caspase-mediated apoptotic tumor cell death.	[43]
SAS tumor.	Comparison of mEHT and mEHT + RT. Tumor size, survival time, and apoptotic signals were measured.	The survival time significantly increased with combined RT + mEHT treatment, and the tumor growth was inhibited.	The increased apoptosis and survival time indicate the excellence of the mEHT + RT treatment.	[44]
C3H/He mice inoculated with SCCVII to the left femoral and in the chest region. Dendritic cell immune stimulation was applied.	mEHT 42˚C 30 min, Flow cytometry, immunohistochemistry, CD3+, CD4+ and CD8+ immune-cell detection.	The CD8+ and S100 were more strongly expressed in the DC plus mEHT treatment group than in control or stand-alone therapies, although Foxp3 expression was much higher in the control group.	A significant abscopal effect was measured between the treated femoral and untreated chest regions of the mice. The local treatment also became a whole-body immune attack on the metastatic lesions.	[45]
BxPC-3 human pancreatic adenocarcinoma xenograft.	mEHT treatment compared to control the tumor size is measured and compared to sham (10-10 mice).	The tumor sizes were significantly reduced, and mEHT inhibits the growth.	The mEHT significantly responds to mice in the resistive, aggressive pancreatic tumor.	[14]
4T1 cells were orthotopically injected into Balb/C mice.	Variants of liposomal doxorubicin were compared, and the release of the drug and the mechanism of the cell distortion were measured.	The mEHT treatment significantly promoted the release of the drug in the locally treated volume, the highest rate was with LTLD.	The mEHT treatment helps target the tumor with liposomal doxorubicin.	[46]

Continued

A549 xenograft injected into the flank of Balb/C mice.	RT + mEHT expression profile of nuclear receptors NR4A3 and KLF11.	That NR4A3 and KLF11 are critical for increasing the efficacy of radiotherapy combined with mEHT.	The study identified the molecular mechanism to sensitize lung cancer to RT + mEHT.	[47]
OVCAR-3, SNU-17, PDTX-19 cell lines treated with mEHT.	Tumor volume was studied in the time course. Cell number and Western blot were compared for mEHT and wHT 24 and 48 h after treatment.	The superiority of mEHT is observed in all cases; the difference between mEHT and wHT increases over time. The addition of 3-methyladenine (3-MA) increased the effects.	mEHT induced the death of ovarian and cervical cancer cells through apoptosis, and its anticancer effect was enhanced by inhibiting mEHT-induced autophagy.	[48]
9L glioma tumor allograft.	Tumor tissue oxygenation level was measured using an O2-sensitive electrode system. Standard 42˚C 30 min mEHT.	Oxygen level was significantly higher (almost double) in the treated tumor than before.	mEHT substantially increases the oxygen level in tumors in 9 L gliomas in rats.	[49]
Companion animals (dogs and cats) with tumors) treated with mEHT.	Natural tumors of dogs were treated after failure of conventional (surgery and chemotherapy) treatments.	Significant shrinking of tumors (even lung metastasis) was achieved together with improved quality of life of the animals.	The mEHT is a valuable tool for veterinary oncology and gives stable information for human clinical applications.	[13]

Most treatments were made on rodents. However, the thermal efficacy was measured *in vivo* on a healthy female pig (49.5 kg) liver, which is a model of a deep-seated, highly blood-perfunded organ [35]. The tumor focus was unavailable without the tumor in the liver, but the focus on the liver in the large-sized experimental animal was proven. The temperature dynamically grew in the liver mass while its surrounding temperature was behind (**Figure 3**). The results show that mEHT can thermally impact the liver without raising the skin temperature; no surface overheating was observed, and the skin and the fatty tissue remained in a safe heating regime. Anesthesia influences temperature development in a short time. The physiological control actively regulates thermal homeostasis, having isothermal heating in the liver, while in a deep anesthetic state, the regulation is slower and less effective. The step-up heating condition in deep anesthesia allows for weaker physiologic reactions, making thermal regulation (**Figure 3(C)**).

The temperature development was measured in various experimental setups [50]. The typical temperature measurements in mice and dogs show good deep heating focus (**Figure 4**) Noteworthy is the temperature in the lung (**Figure 4(D)**), which is well distinguishable high despite the cooling by the animal's breathing **Figure 4(D)**. The power started high, but keeping the temperature enough was a fraction of the initial value because keeping the temperature only replaces the "lost" heat caused by the environmental conditions. Various treatment setups and tumor sizes influence temperature development, and the starting power is decided for the initial slope of the temperature plot.

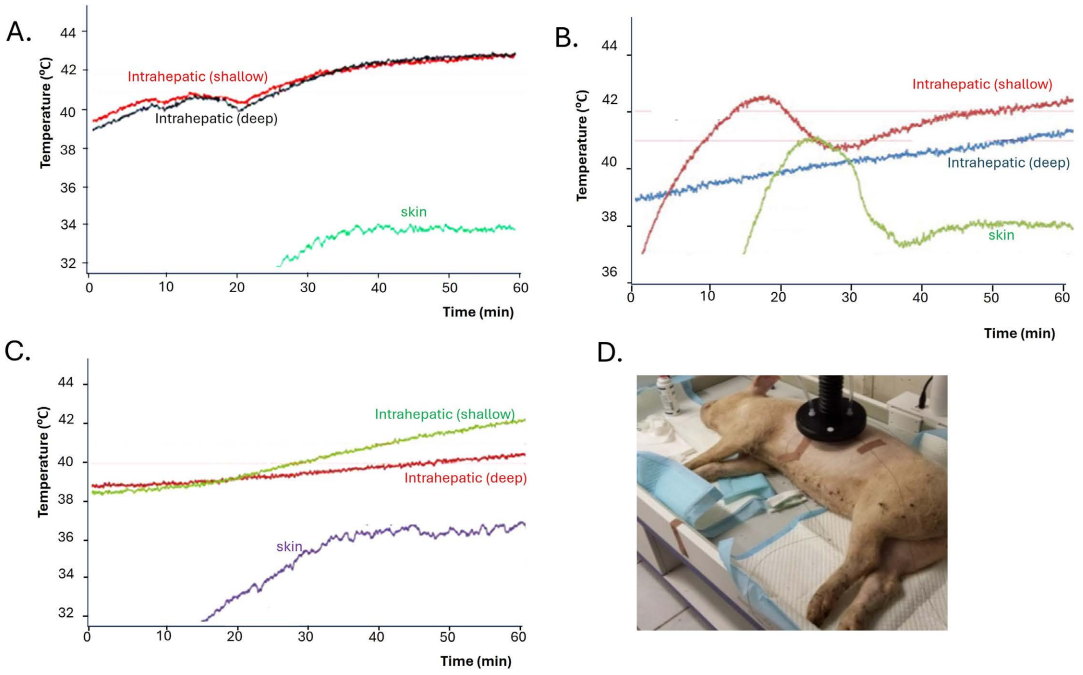

Figure 3. Temperature measurement in the liver of a healthy pig (42˚C, 60 min, 150 W max.) (A.) The permanent 150 W power treatment was started 10 min after anesthesia. (B.) The permanent 150 W power treatment was started 30 min after anesthesia. (C.) Step-up heating treatment from 60 W to 150 W. (D.) The anesthetized animal during the treatment.

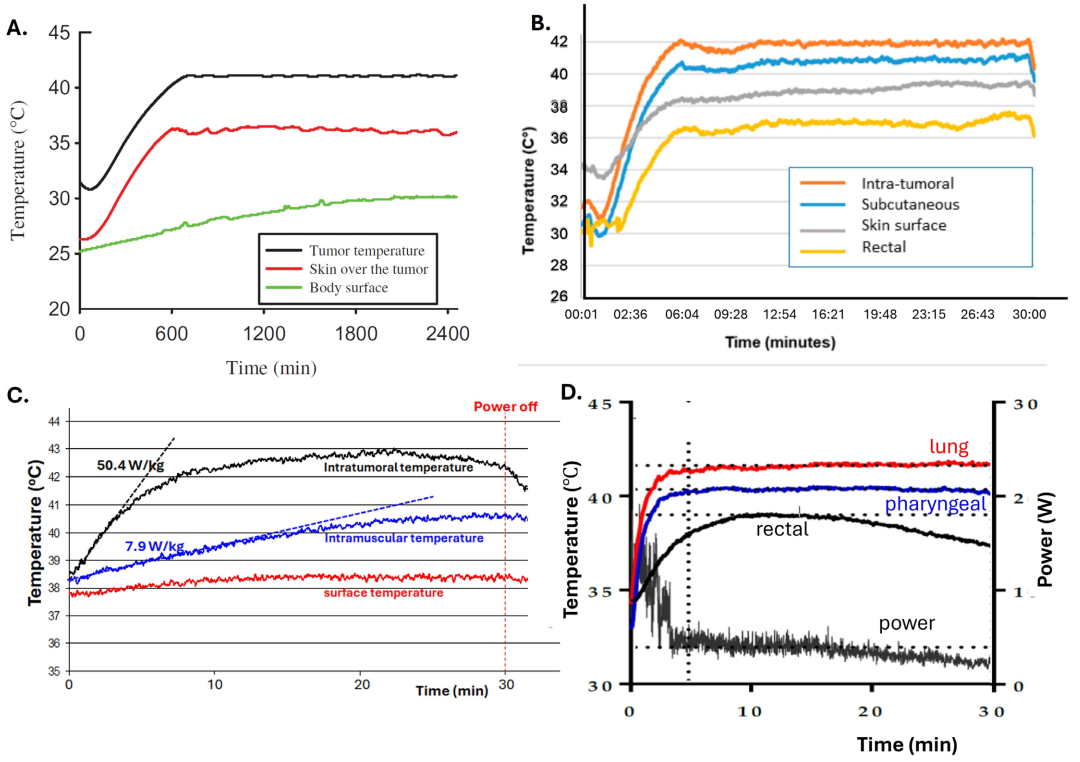

Figure 4. Typical temperature measurements (A.) FSall fibrosarcoma [18], (B.) B16F10 melanoma [30], (C.) Recurrent epithelial cell carcinoma of the lower neck region of a bull-terrier [50], (D.) B16F10 pulmonary melanoma metastasis [42].

The intratumoral temperature is usually fixed in the protocol for 42℃,(30 min treatment time), but the extratumoral temperatures vary by the animal, the tumor, and the environment Figure 5.

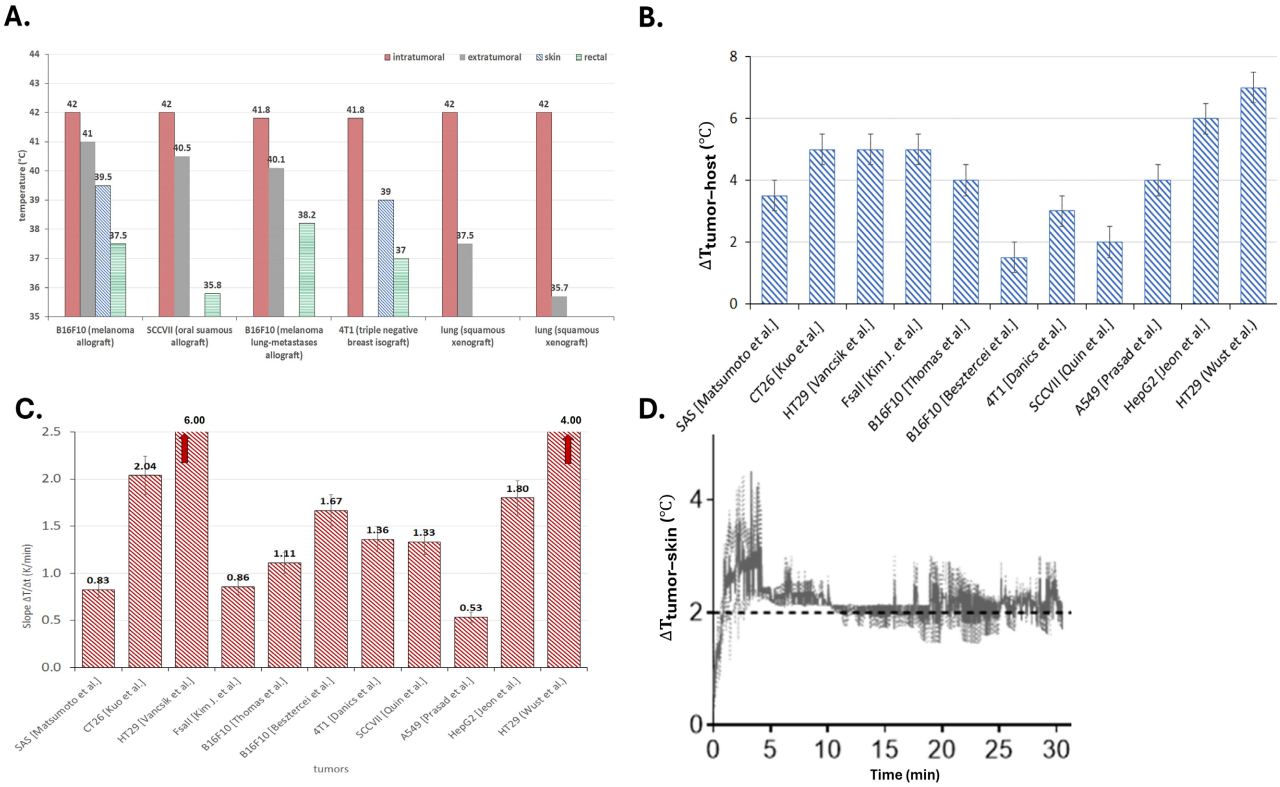

Figure 5. The thermal conditions of the various experiments. (A.) The temperature values are in different sensor locations: B1610 [30], SCCVII [45], B1610 metastasis [42], 4T1 [20], and lung squamous [33] [39]. (B.) The temperature difference between the tumor core and its surroundings: SAS [44], CT26 [29], HT29 [26], FSall [18], B16F10 metastasis [42], B16F10 [30], 4T1 [20], SCCVII [45], A549 [32], HepG2 [21], HT29 [37]. (C.) The time derivative of the temperature measures the dynamics of the temperature growth. (SAS [44], CT26 [29], HT29 [26], FSall [18], B16F10 metastasis [42], B16F10 [30], 4T1 [20], SCCVII [45], A549 [32], HepG2 [21], HT29 [37].) (D.) The skin temperature was 3˚C lower than the intratumoral, but with thermal homeostasis, it stabilized on 2˚C difference [20].

The thermal component of mEHT heats the target. When the power adjusted step-up for a longer time (~1000 s) from 1.5 W to 2.5 W, the steady temperature growths proportionally reaching 42˚C in the tumor and ~33˚C in nearby tissues after 1000 s, when the power is downregulated to 2 W [33]. This high difference between the tumor and host temperatures is caused by the cooperative changes with thermal homeostasis and relatively high cooling, which requires 2 W power to keep the temperature constant. These special conditions were used for temperature mapping in a murine model, which agrees well with the simulations. In humans, the efficacy of mild temperature hyperthermia was studied in cervical cancer, which increases the peritumoral temperature to 38.5˚C, with proper blood flow for the complementary treatments [51]. The synergy of thermal and nonthermal processes induced by mEHT destroys the tumor, Figure 6.

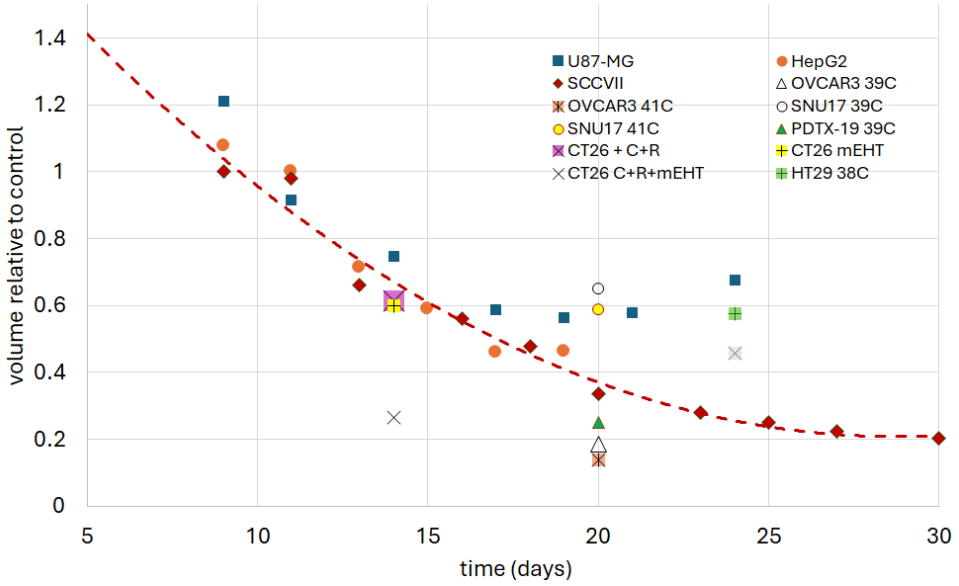

Figure 6. The tumor volume relative to control was measured in various tumors in different publications. (U87-MG [22], SCCVII [45], HepG2 [21], OVCAR [48], SNU17 [48], PDTX-19 [48], CT26 [29], HT29 [40].)

The tumor inhibition by oncothermia on human pancreatic adenocarcinoma cell line (BxPC-3) in female CD-1 mice (10-10 animals are involved). On Day 72, mice were sacrificed, and their tumors were excised and weighed. A significant difference was observed in the total weight of excised tumors between the control and treated groups. In summary, there were a total of ten treatment doses administered to each mouse (six doses in cycle 1 and four doses in cycle 2) using oncothermia [14], **Figure 7**. The mice responded well to the treatments, and no adverse side effects were observed. The treatment does not change the average body weight of mice. The tumor growth inhibition was 66% after the second cycle ($p < 0.0005$) measured on excised tumor weights.

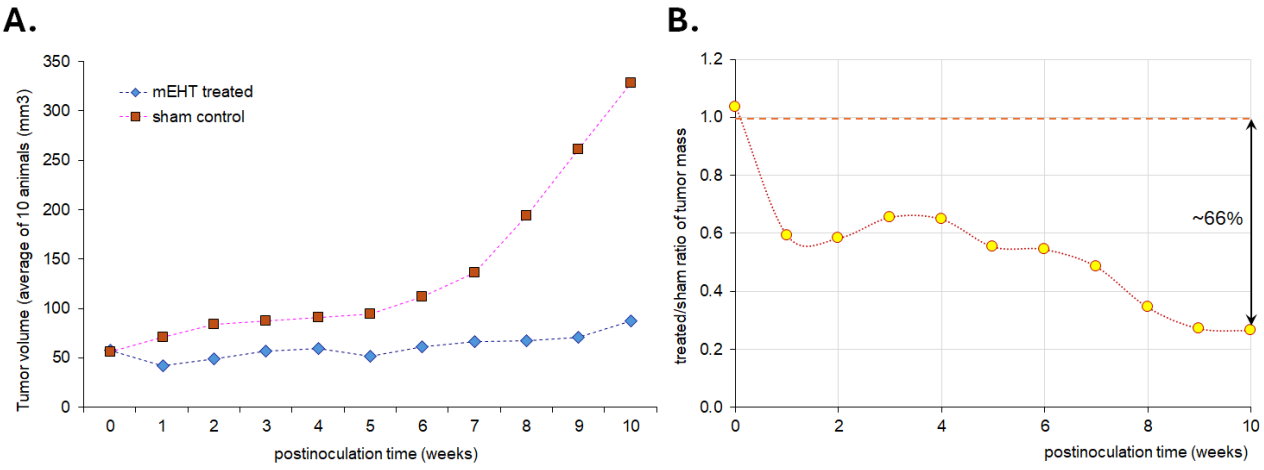

Figure 7. The pancreatic adenocarcinoma (BxPC-3) xenograft experiment [14]. (A.) The tumor volume of the treated and sham control is from the inoculation of the cancer cells. (B.) The ratio of mEHT to sham shows significant growth inhibition.

It is noteworthy that the suppression of the tumor volume may be observed at temperatures as low as 39˚C. Figure 8, measured in gynecological (ovary and cervix) tumor models. The tumor volume was significantly below the control in all cases.

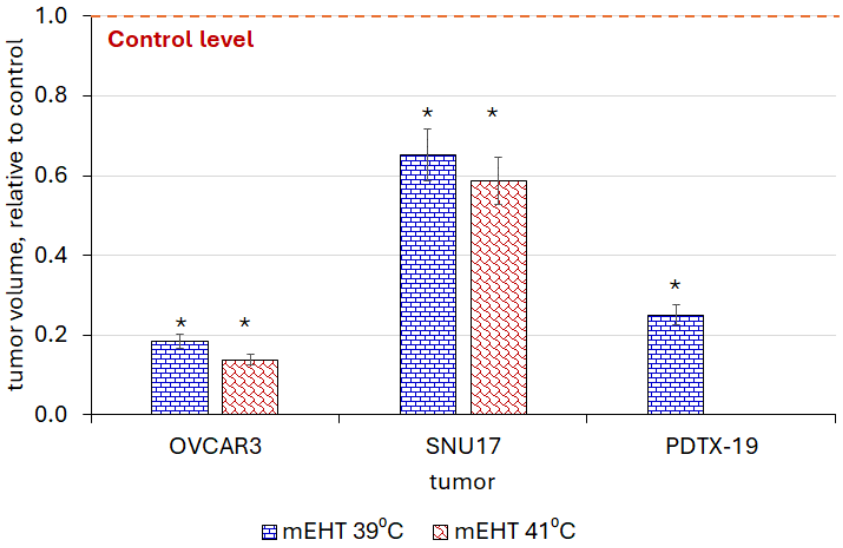

Figure 8. Temperature as low as 39˚C significantly suppresses the volume of ovarian (OVCAR-3) and uterus cervical (SNU-17, PDTX-19) tumors compared to the control in the athymic nude mice model. A 2C temperature increase reduces the tumor volume by 25% and 10% in OVCAR-3 and SNU-17 tumors, respectively [48]. The reference control is shown with a dotted line at 1.

Obtaining information about the synergy of thermal and nonthermal effects needs infrared heating [40] instead of the inapplicable water bath, which was *in vitro* a plausible pure thermal reference. The nonthermal addition to the thermal basis (42˚C) increased the dead tumor part ≈ 4.3 times larger than the only thermal effect in HT29 colorectal carcinoma [40], Figure 9. It is noteworthy to check that the nonthermal component, the difference between the mEHT treatment and control, both at 38˚C, shows a missing value to the mEHT 42˚C results are about the same as those of the measured thermal effect alone.

Apoptotic cell death dominates tumor cell destruction with intensive development of apoptotic bodies, Figure 10. The volume of apoptosis depends on the treatment time and rapidly grows by the posttreatment time of the mEHT. The tumor destruction ratio (TDR, %) differs between the treated and distant, nontreated tumors. Notably, the dead area in the nontreated tumor decreases over time, while the treated tumor increases it. The ratio of the dead areas became constant from 48 h to 72 h, making the distant tumors' interaction probable over time. In the early stages, the mitochondrial changes (decrease of membrane potential and opening transition pores); in the late stages, the caspase activation nucleus karyopycnosis, loss of cell membrane integrity, and DNA fragmentation occur.

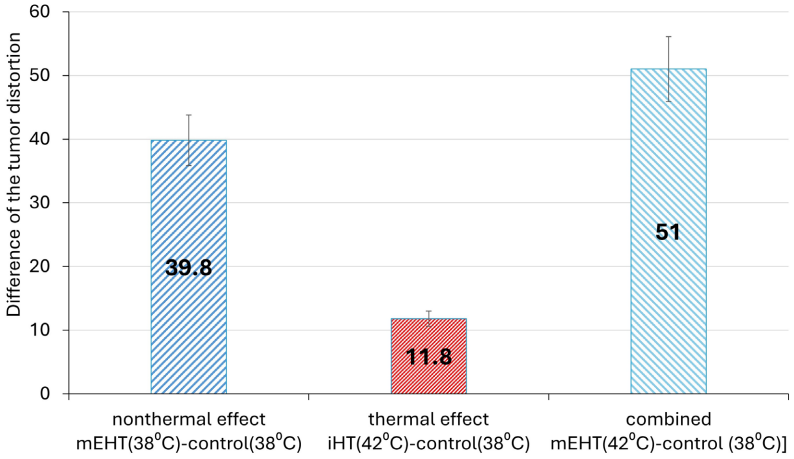

Figure 9. The comparison of thermal (infrared heating, iHT) and combined thermal and nonthermal (mEHT) effects relative to control [40]. The mEHT was done in temperatures of 38˚C and 42˚C, the sham control at 38˚C and the iHT at 42˚C. The comparison of sham and iHT shows the pure thermal effects and the mEHT (38˚C to sham the pure nonthermal. The sum of thermal and nonthermal components gives the combined effects, which was measured with mEHT at 42˚C, indeed.

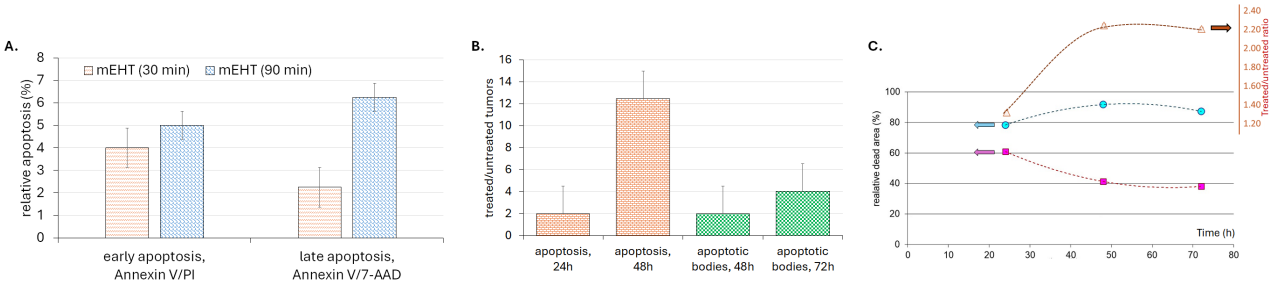

Figure 10. The apoptotic ratio of treated tumors. (A.) Early and late apoptosis (measured with Annexin V/PI and Annexin V/7-AAD, respectively) in B16F10 lung metastasis of melanoma in mice registered 24 h after treatment [42]. (B.) Late apoptosis and apoptotic bodies 24 h and 48 h after treatment of HT29 xenograft in mice [52]. The ratio of the treated and non-treated tumors in the same animals is shown. (C.) The development of the dead area (%) is treated and nontreated tumors on the same mouse [52]. The ratio of the percentages is shown in the secondary axis. The lines are guiding for the eye.

The stress-induced antiapoptotic chaperones HSP70 and HSP90 are exhausted in the cytosol [20] and turn proapoptotic by relocating to the membrane and expressing in the tumor microenvironment (TME). The internal HSPs (iHSPs) exhaustion is connected to the subsequent cell destruction (**Figure 11**). The shifts in the time course points of different tumor entities could be only the effect of the discrete point measurements (**Figure 11(A)**). The iHSP90 has its maximum much earlier than the iHSP70 (**Figure 11(B)**), and TDR follows the iHSP expressions in their baseline return [20] (**Figure 11(C)**). The identical dynamism of the destruction and cCas-3 shows the dominance of the caspase-dependent apoptotic pathways in 4T1 tumors [20]. Notably, the significant development of chaperoning iHSPs was a few hours posttreatment, indicating that the combined stress of the mEHT treatment excited intracellular processes, which induced the chaperone activity.

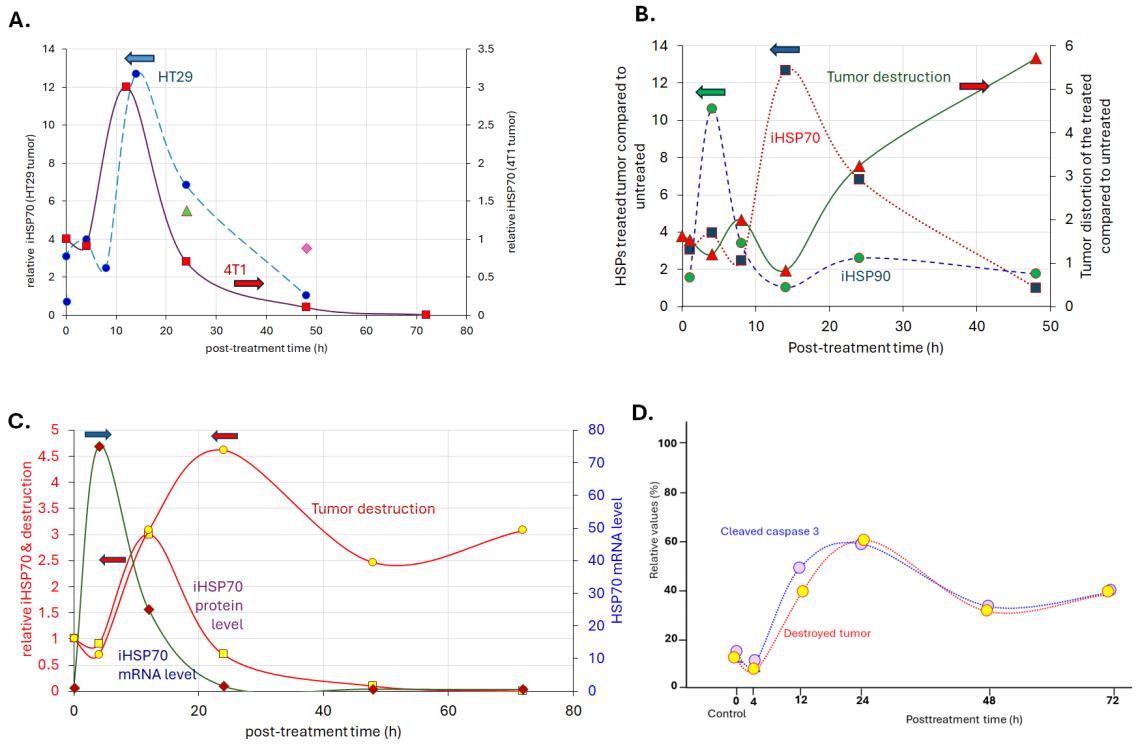

Figure 11. The HSP chaperons and the cell destruction by time-course experiments. (A.) iHSP70 development in HT29 [24] and 4T1 [20] tumors. Other measurements in single time point 24 h (4T1 tumors, ▲, [43]), and 48 h (B16F10 tumors, ♦, [30]) are also shown. (B.) The progressing dynamism of iHSP70 and iHSP90 with cellular distraction [23] [24]. (C.) The iHSP development in mRNA and protein levels was followed by the destruction of the 4T1 tumor [20]. (D.) the cCas-3 and the tumor-destruction dynamisms are identical [20].

The gene study 4 h post-mEHT (42˚C, 30 min) treatment of HT29 tumor xenograft showed significant differences between the wHT and mEHT at the same 42˚C temperature, and both significantly altered from the sham control [24] (**Figure 12**). The mEHT mostly upregulates the expression of iHSPs at the mRNA level. The HSPA1A, HSPA6, and HSPA8 genes encode various HSP70 family members (proteins 1A, 6, and 8, respectively). The HSPD1 and HSPH1 genes encode HSP60 and HSP105 chaperons, respectively. The death receptor D6 (TNFRSF21) is upregulated, and the surface receptor activator of osteoclasts, RANK (TNFRSF11), as well as Calpain 1 and 9, which support the cell autonomy and defecting the cytoskeleton, are downregulated. The BAG gene encodes the cochaperone of HSP70, and the EGR1 gene encodes a transcription factor protein, which is involved in multiple upregulated apoptotic processes. In general, we conclude from the gene map analysis that the mEHT strongly supports the apoptosis of the selected tumor cells and destroys the tumor "softly". Nonnecrotic destruction helps liberate undeformed intracellular information from the dying cell, which could trigger antitumoral immune processes. Some other gene mapping [21] [22] [43] strongly support the above observations *in vivo*, which was also seen *in vitro* [53]. The gene map shows a distinct difference in the gene regulations between the homogeneous wHT and inhomogeneous mEHT treatment sat the same 42˚C temperature. Injection of NR4A3 or KLF11 siRNA into

mouse A549 lung xenograft tumors knock down the effectiveness of RT and its combined application with mEHT [47], revealing some aspects of the mechanism of sensitization of A459 tumors for RT and mEHT in xenograft experiments.

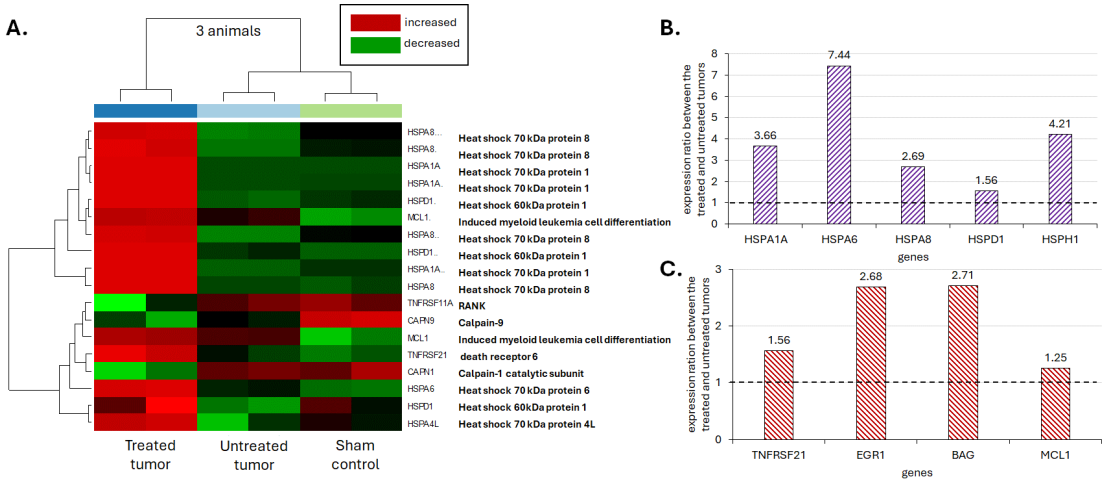

Figure 12. The mRNA gene chip results from some primary players of the mEHT effect. (Affymetrix 3' IVT Express Kit (Affymetrix, Santa Clara, CA, USA). Samples were hybridized on HGU133 Plus2.0 arrays [24]. Pooled samples from 3 animals. (A.) The massive upregulation of iHSPs and death receptor D6 together with the proapoptotic MCL1. (B.) The values of the up regulation of iHSP genes. (C.) Some other up regulated genes help the apoptotic processes.

The protein expression (Proteome Profiler Human Apoptosis Kit) of HT29 tumor in xenograft experiments, 8 h, 14 h, and 24 h after mEHT treatment (42˚C, 30 min) shows many proteins, including pro and anti-apoptotic sets. 8 h posttreatment, the transmembrane excitation of the extrinsic pathway shows an increase of TRAILR2/DR5 and FAS-FADD complex and enhanced expression of antiapoptotic proteins, which activity drastically reduced at 14 h and further at 24 h posttreatment observations. The catalase protein remains active after 24 h, which probably regulates ROS production to the level necessary for proper apoptosis to avoid necrosis. All other proteins remain under the reference level after 24 h posttreatment of HT29 xenograft measurement (**Figure 13**) [52].

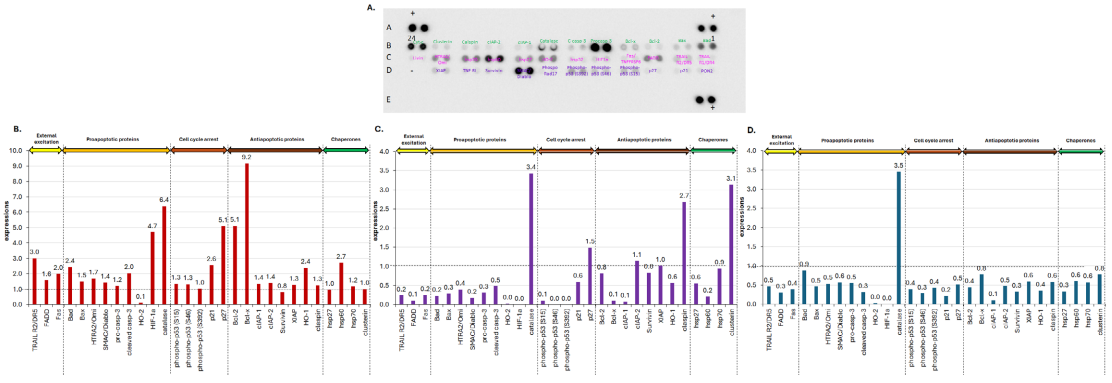

Figure 13. Relative expressions of proteins play a majority role in apoptotic processes [52]. The baseline is shown with dashed lines at 1. (A.) The matrix of the Proteome profiler human apoptosis kit array. (B.) 8 h after mEHT treatment. (C.) 14 h after mEHT treatment. (D.) 24 h after mEHT treatment.

The cyclin-dependent kinase (CDK) inhibitors p21 and p27 are highly activated in the first 6 h after mEHT treatment and assist apoptosis by acting at different stages of the cell cycle as checkpoint controllers under the regulation of the p53 tumor-suppressor protein. The p27 CDK remains activated at 14 h post-treatment, preventing premature DNA synthesis. When the cell encounters stress like DNA damage, p53 becomes activated and plays a critical role in deciding cell fate. It can trigger cell cycle arrest to allow for DNA repair or initiate apoptosis (programmed cell death) if the damage is too severe. The activated p53 may trigger apoptosis by initiating proapoptotic genes and inhibiting antiapoptotic genes. The base form is the unphosphorylated p53 protein, which has modifications by the phosphate group (PO_4) bonded to serine (S) amino acids at positions 15, 46, or 392, modifying its regulatory mechanisms. Phospho-p53 (S15) increases the p53 protein stability and enhances the ability to bind to DNA and activate its target genes. The phospho-p53 (S46) promotes apoptosis, and the phospho-p53 (S392) is involved in transcriptional activation and potentially modulates its role in cell death pathways independent of transcription. The mEHT treatment significantly increases the expression of p53, p21, and p27 proteins in various tumors of treated mice, while the wHT effect is moderate, Figure 14.

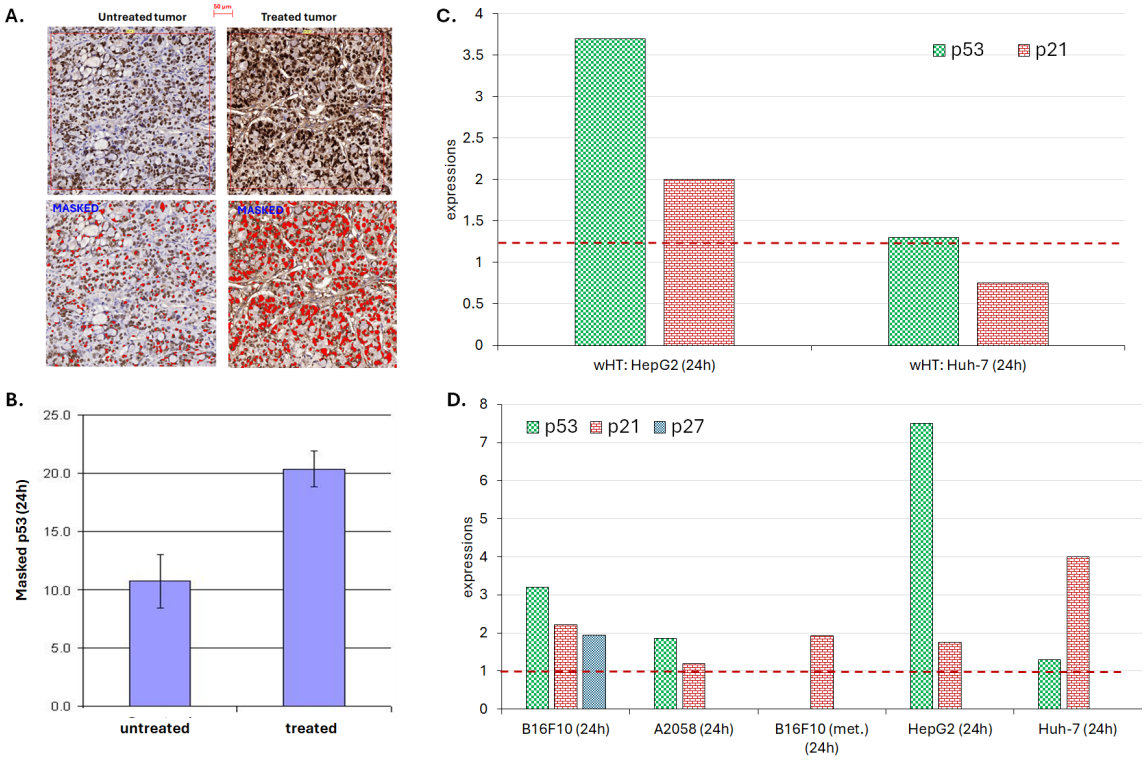

Figure 14. The expression of p53, p21, and p23 proteins in various tumor types. (A.) Immunohistochemical pattern of p53 protein 24 h after treatment on HT29 xenograft [54]. (B.) The masked p53 was significantly higher in the treated tumor than the untreated one in the same animal [54]. (C.) Development of p53 and p23 proteins 24 h after wHT[21]. (D.) Expressions of p53, p21, p27 proteins in various tumors 24 h after the mEHT treatment. (B16F10 [30], A2058 [28], B16F10 metastasis [42], HepG2 [21], Huh-7 [21]).

The mEHT extrinsically excites pathways for apoptosis [4] [55]. The extrinsic signal starts in the TRAIL death receptor with FADD and FAS complexes [38]. The TRAIL signaling, as usual in complex systems, has a dual effect, being pro-or antitumoral, depending on the TME conditions [56]. The membrane fluidity increases due to thermal effects [57]. Investigating the thermal and non-thermal complexity of apoptosis shows that the mEHT excites numerous apoptotic pathways in the cell, **Figure 15**. The optimally modulated carrier signal directs the TRAIL to be proapoptotic. Massive apoptosis is noted with mEHT treatments, likely following the caspase-dependent extrinsic signal pathway with Caspase-8 (Cas8). The path may split towards the Cas3 followed by apoptosis (Cas8 → Cas3 → apoptosis), or to mitochondria by signal transfer of BID protein. Mitochondria may ignite the intrinsic signals for apoptosis [20]. The intrinsic path has two options: it could be caspase-dependent (through Cas9), involving apoptosis-inducing factor (AIF) [23] [58]. AIF is usually located in the mitochondrial intermembrane space, but it is translocated to the nucleus, generating chromatin condensation and DNA degradation, providing an additional signal pathway for apoptosis. This process has the potential to affect untreated tumors as well. A notable factor is the arrest of the XIAP effect to block the main path of caspase-dependent apoptosis by the secretion of SMAC/Diabolo [38] and Septin4 [21]. The ignited nonthermal chemical processes are massively gained by the thermal conditions, producing a complex network resulting in

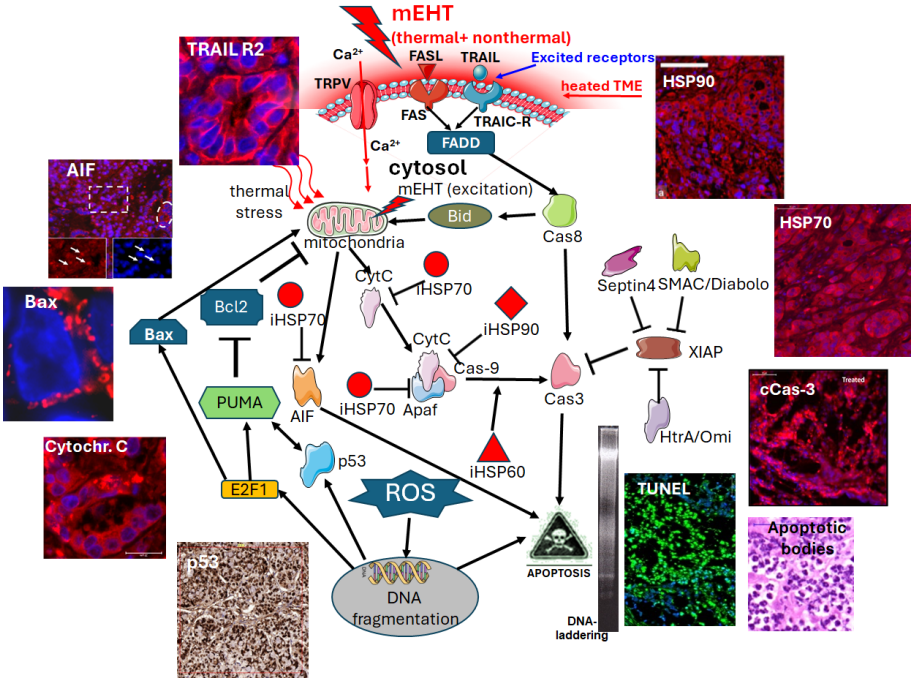

Figure 15. The mEHT excited apoptotic pathways. Some immunohistochemical results are shown around [23] [24] [52]. The main apoptotic pathways, without detailed molecular involvements. Multiple pathways may cause apoptosis after the mixture of thermal and non-thermal energy absorption. The protective mechanisms of intracellular HSPs exhausted, and the network of multiple possible pathways executes the apoptotic process.

apoptosis. Thermal stress strongly supports the intrinsic apoptotic pathway through BAX and cytochrome c (point of no return), finishing the apoptosis through the cleaved Cas3 (cCas3) path. DNA fragmentation drives tumor-cell degradation [59]. The induced stress by mEHT upregulates the tumor suppressor p53 protein, one of the key cell-cycle regulation and DNA repair players. The p53 "master switch" drives the DNA fragmentation and the appearance of apoptotic bodies.

Noteworthy that mEHT also destroys the tumor stem cells in the U87-MG and A172 human glioma cells inoculated into BALB/c nude mice xenograft [22].

The appropriately chosen modulation may trigger resonant excitations of the transmembrane proteins, excite the TRAIL R2 (DR5) death receptor, and activate the apoptotic pathway. Despite the increased expression of iHSPs, the mEHT inhibits tumor growth and supports apoptotic processes [25]. The expression of HSP70s has its maximum at around 12 h posttreatment. The extremely large complex thermal and non-thermal stresses exhaust the HSP protective response [20]. The intracellularly overproduced antiapoptotic HSPs relocate to the cell membrane or are released to the TME. The exhausted HSPs cannot block the apoptotic process [20]. Another antiapoptotic protein, the XIAP, is arrested by Septin-4 [21], SMAC/Diabolo, and HTRA-2 proteins in HT29 xenograft treated with mEHT 42˚C 30 min. [52]. The development of the primary components was measured by immunohistochemistry of resected tumors of the sacrificed animals, **Figure 16**.

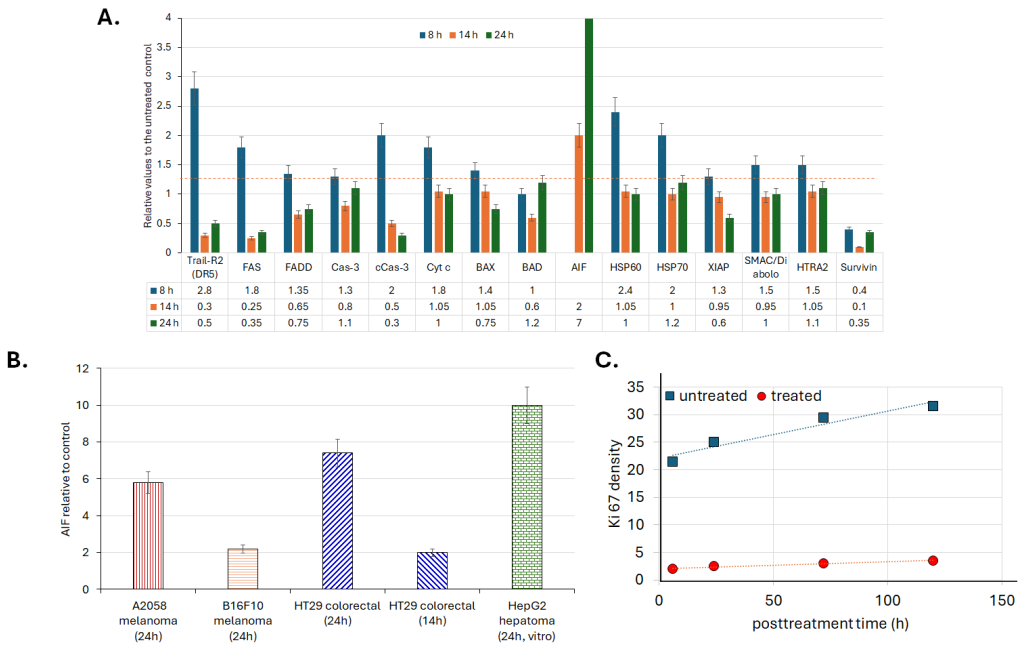

Figure 16. Mayor molecules are involved in the mEHT-induced apoptotic process. (A.) The development is shown 8 h, 14 h, and 24 h after treatment in HT29 xenograft [52]. (B.) The caspase-independent AIF pathway in A2058 [28], B16F10 [30], HT29 [23], and HepG2 (*in vitro* [60]) tumors. The Ki67proliferation marker protein, expressed in the nuclear membrane only in the dividing cells, is strongly suppressed (about one order of magnitudes) by mEHT in rat glioma (L9) [49].

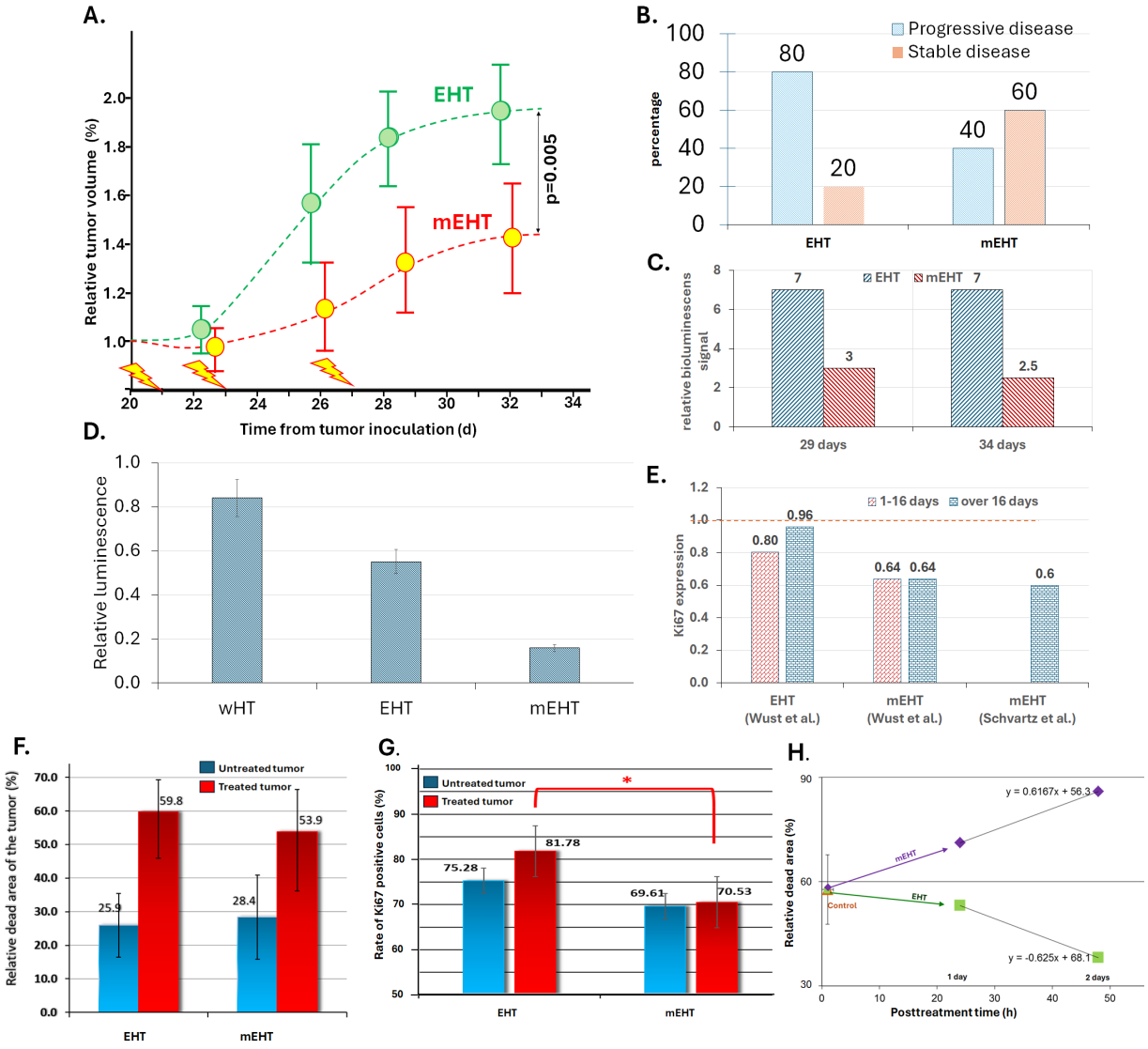

Figure 17. Effect of modulation in mEHT treatment [37]. (A.) Changes in relative tumor volume after inoculation of HT29 tumor. After 5 days of the last (3rd) treatment, the difference became significant between tumor distraction by EHT and mEHT. (B.) The development of the diseases also favors modulated treatment. (C.) Between the 29th and 34th days, the dereference is stabilized. Compared to wHT, the unmodulated EHT has the advantage of tumor growth measured by the non-invasive bioluminescent method. (E.) The Ki67 proliferation marker is significantly suppressed in mEHT compared to EHT, which is proven by 4T1 tumors [43], too. (F.) The modulation effect in mice with double-distant C26 colorectal tumors inoculated in the two femoral regions. The right side was treated while the left was regarded as a control [65]. (G.) The Ki67 proliferation marker significantly decreases with the treatment in both (treated and untreated) tumors of the same mouse [65]. However, the modulation has no significant difference from the unmodulated one in C26 tumors. (H.) The relative dead area in the middle cross-sections of the isolated tumor was taken from both sides after treatment on only one side. The difference became obvious by the elapsed time: the treated tumor shrank further, increasing the dead area, while the untreated grew in HT29 tumors [66].

The amplitude modulation of the carrier frequency signal (13.56 MHz) increases the effective value of the electric field of mEHT. It supports the cytoskeleton's polymerization and the reorganization of the cytoskeletal network. Cytoskeletal polymerization has a significant effect on cancer cells, which inhibits

cellular plasticity and cell migration. The $1/f$ fractal noise modulation introduces a huge amplitude increase at the carrier frequency, increasing its selective excitation facility. The noise modulation approach is like the harmonizing method [61], whose application is emerging in physiology [62]. The modulation may promote the execution of the enzymatic processes [63], modifying the transition between the initial and final states of molecules [64]. The applied modulation orchestrates the spatiotemporal order of the exported molecules to the TME and may trigger resonant excitations of the transmembrane proteins and extrinsically excite signal pathways for apoptosis. The benefits of modulation appear compared to the unmodulated (EHT) treatments (**Figure 17**). [37] Modulation experiments with the mice having two distant tumors in their femoral regions also show the advantage of the modulation [65] [66], **Figure 17(F)**, **Figure 17(G)**, **Figure 17(H)**.

The pulsing modulation pattern further improves tumor destruction [19], **Figure 18**. The pulsed signal significantly increases apoptosis (suppresses the Ki67 proliferating marker), decreases the growth rate, and develops fewer antiproliferative iHSP70 chaperones.

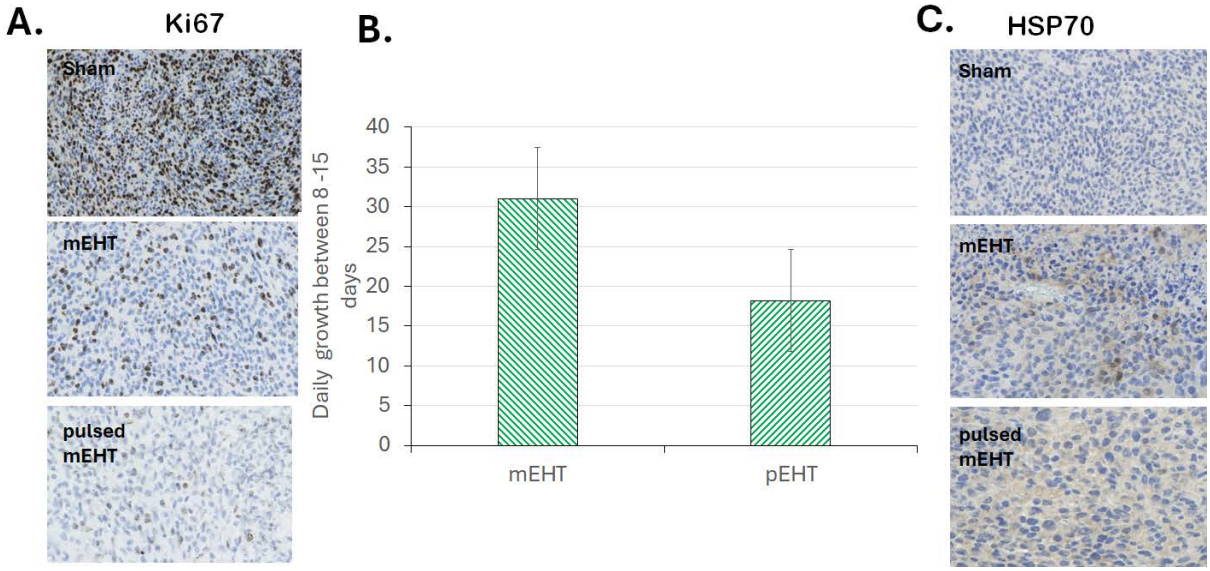

Figure 18. Effect of pulsed modulation measured in RG2 (D74) glioma is Fisher rats [19]. (A.) Ki67 proliferation marker. (B.) The growth of the tumor between 8 - 15 days. (C.) Development of the iHSP70 in different treatments.

The thermal component of mEHT acts in synergy with the electric excitation, affecting the repair of DNA. The induced upregulation of cyclin-dependent kinase inhibitor protein ($p21_{waf1}$) and the reduced Ki67 proliferation marker correlates with the expression of the $\gamma H2AX$, which is a sensitive molecular marker of DNA damage, **Figure 19**. When p27 was unsuccessful in inhibiting premature DNA synthesis, the double-strand break (DSB) in DNA (shown by the $\gamma H2AX$) leads to apoptosis in mEHT-treated tumors [30] [42]. mEHT activates DSB production.

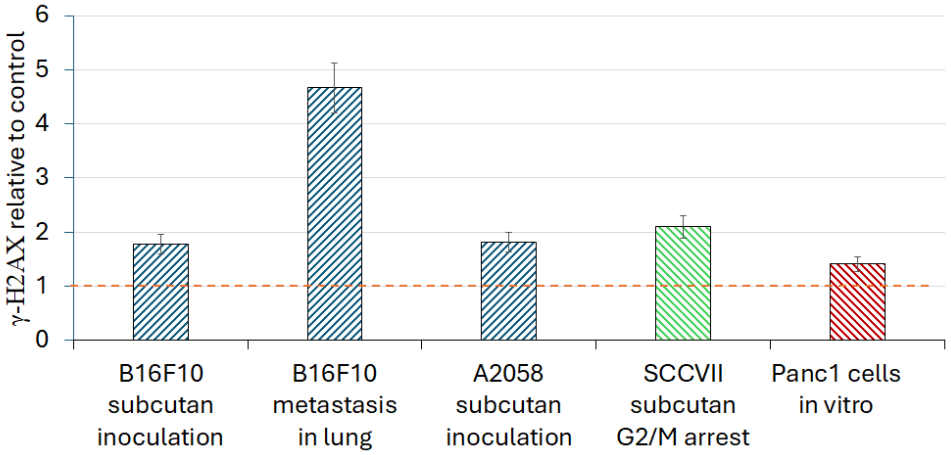

Figure 19. The relative expression of the $\gamma H2AX$ in various tumors developed by inoculation of cancer cell lines. The reference level is 1, indicated by a dashed line. (Subcutaneous B16F10 [30], metastatic B16F10 [42], subcutaneous A2058 [28], subcutaneous SCCVII [45], and Panc1 (*in vitro*) [67]).

DNA damage by DSB could be promoted with an ionization beam of RT in complementary applications with mEHT. The TDR with RT + mEHT combination shows a significant decrease. The tumor volume increase is inhibited more in combined treatment than in standalone treatments, and survival decreases most rapidly in combined therapy of mice [44], **Figure 20**. The only thermal treatment with RT (RT + wHT) does not show the same inhibition of tumor growth as the RT + mEHT does.

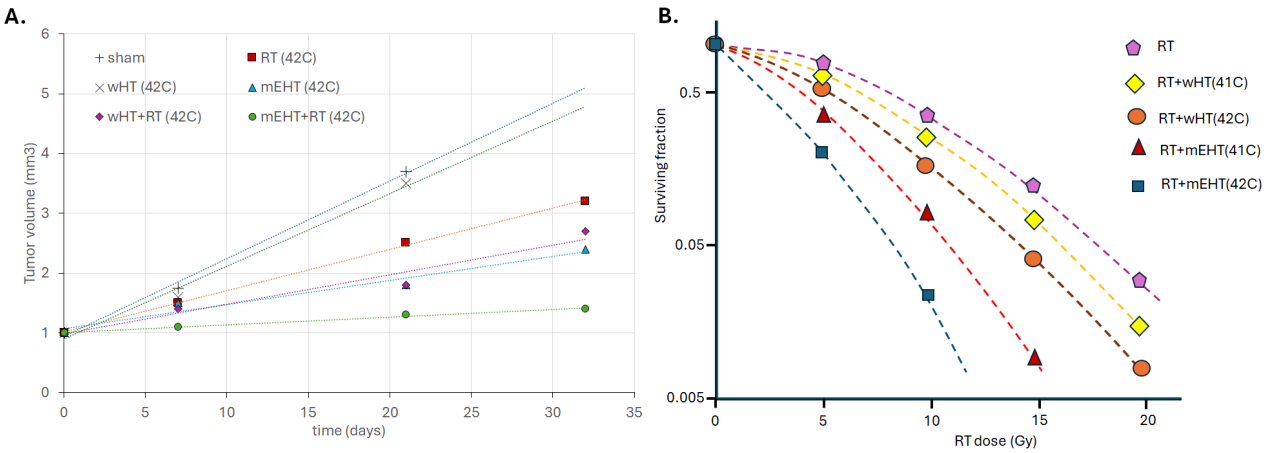

Figure 20. Growth inhibition with complementary RT + mEHT treatment combination for mice having tumors by inoculated SAS cancer cells. (A.) The RT + mEHT combination slows the growth of tumor volume. The tumor volume practically did not change in 32 days after treatment, while RT alone or its combination with wHT had 2+ times higher growth rate. (B.) The surviving fraction of various treatment modalities shows the superiority of RT + mEHT.

The equivalent dose for apoptosis was determined [32] in **Figure 21** for tumors of A549 and NCI-H1299 cells in BALB/c nude mice in a xenograft experiment. The amount of apoptosis was the same with RT and mEHT on tumors by

inoculated A549 cells five days posttreatment (mEHT standard before RT (42˚C, 30 min)/session, RT standard 5 Gy/fraction, daily 2 times). The equivalent dose calculation used the *in vitro* determination of linear-quadratic equations from cell survival curves at standard RT + mEHT treatment: $\alpha_{A549}=0.5318$, $\alpha_{NCI-H1299}=0.5141$, and $\beta_{A549}=0.0283$, $\beta_{NCI-H1299}=0.0163$. The α value *in vivo* linearly depends on the temperature with a slope 0.005 $\frac{1}{Gy\cdot^{\circ}\mathrm{C}}$, starting from $\alpha=0.056$ at 40.5˚C. The apoptosis relative to the control did not show differences between the standard RT and mEHT treatments, but their combined treatment showed ~20+% more apoptosis than the addition of the two independently obtained values (Figure 21(A)), which supports that the combination is not additive but synergetic. The mEHT equivalent changes by temperature, starting with 20 Gy at 37˚C and almost doubling to 42˚C (Figure 21(B)).

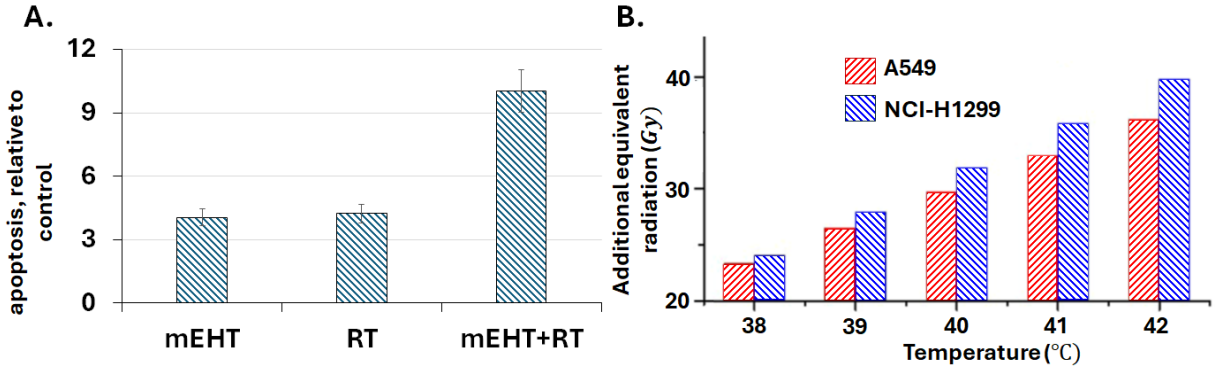

Figure 21. The equivalent dose determination [32]. (A.) Apoptosis measurement compared to the control. (B.) The equivalent radiation dose to addition to 20 Gy at 37˚C baseline.

The measurements of oxygenation (pO_2) before and right after the mEHT treatment showed a 78% increase in the pO_2 value on the treated side compared to untreated in Fisher rats with inoculated L9 glioma cell line in double tumors [68]. This increase supports the complementary therapy with RT. The mEHT generally increases blood flow in tumors, as shown in cervix tumors [51], and the higher blood flow increases oxygenation. On the contrary, the RT decreases blood flow due to damaged vessels, consequently increasing hypoxia in addition to hypoxic tumors. Hypoxia activates the hypoxia-inducible factor-1α (HIF-1α) and the homeostatic regulation induces vascular endothelial growth factor (VEGF) to revascularization and could promote tumor recurrence. HIF-1α can interact with the tumor suppressor protein p53, potentially leading to increased p53 activity and downstream pro-apoptotic signaling. While RT (15 Gy) alone upregulated the HIF-1α mEHT with 41˚C, 30 min treatment suppressed it together with the VEGF in FSalltumors of C3H mice [18]. The mEHT promoted the apoptosis of tumor cells and suppressed the tumor growth rate, Figure 22.

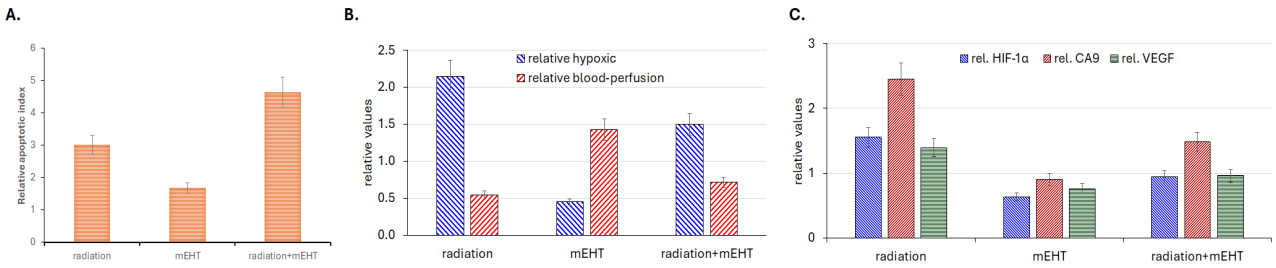

Figure 22. The synergy of RT (15 Gy) and mEHT (41˚C, 30 min) combined application [18]. (A.) Apoptosis, relative to control. (B.) Relative hypoxia and blood perfusion in the targeted tumor. (C.) The relative HIF-1 α , CA9 (Carbonic anhydrase IX, CA9, having a significant role in tumor acidification) and VEGF.

Electrical stimuli increase the penetration of drugs like doxorubicin [69] *in vivo*, and the application of electromagnetic fields has been shown clinically to increase the sensitivity of cells to the effects of chemotherapies such as paclitaxel and doxorubicin [70] [71]. The complementary application of mEHT with chemotherapy improves the cellular destruction of the targeted tumors. The therapeutic effect of thermosensitive liposomal encapsulated doxorubicin (LTLD) was studied in BALB/c mice with tumors inoculated with 4T1 triple-negative breast cancer (TNBC) [46]. The variants of administered doxorubicin (free doxorubicin, (DOX); PEGylated liposomal DOX, (PLD); and LTLD) were compared by their DOX accumulation in tumors after mEHT. The TDR increased significantly by mEHT treatment and further grew by DOX, PLD, and LTLD in that order. The LTLD practically destroyed the complete tumor measured 24 h after the 3rd mEHT treatment. The tumor destruction was massively apoptotic through the cCas-3 signal pathway, which was measured linearly with TDR. The apoptotic process was also indicated by the significant decrease of the Ki67 proliferation marker on the nuclear membrane of the dividing cells [46], **Figure 23(A)**. The LTLD success shows the importance of the thermal effects for thermosensitive liposomes. In another model, murine colon carcinoma-inoculated CT26 cells were measured and treated with only thermal (wHT) and complex thermal and nonthermal (mEHT) effects [34]. While the thermal effects are effective, its synergy with nonthermal processes in mEHT doubles the release of doxorubicin. The mEHT significantly enhanced the uptake of liposome-encapsulated doxorubicin in BALB/c mice. Noteworthy that the liposomal envelope did not release the doxorubicin in the extracellular matrix but was directly liberated in the cytosol of tumor cells, **Figure 23(B)**. In consequence, the tumor growth was significantly suppressed by mEHT, indicating the efficacy of the nonthermal component of the energy absorption. The effect of the thermal factor was earlier also proven by wHT treatment at 39˚C - 40˚C [72].

Other complementary applications with pharma products also show the advantage of the mEHT. The metformin increases the efficacy of mEHT (41˚C) +RT (15 Gy) complementary application in FSall fibrosarcoma in C3H mice. The apoptotic index and cCas-3 grow parallel with the metformin administration, showing the caspase-dependent apoptotic pathway in this tumor [31]. The

metformin suppresses the expression of HIF-1*a*, VEGF and PD-L1, increasing the efficacy of the standalone treatments, Figure 24.

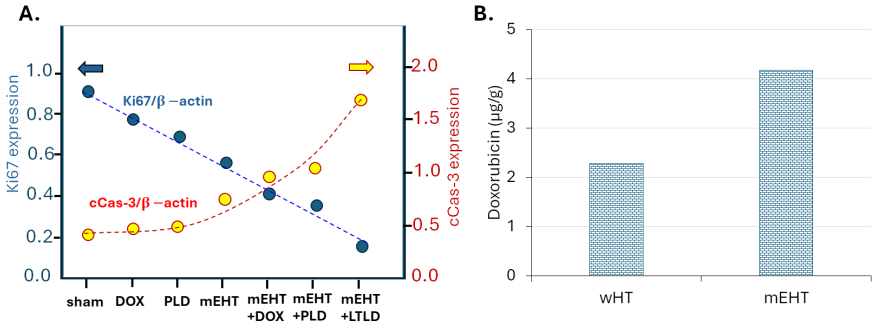

Figure 23. Application of mEHT for liposomal doxorubicin preparations [34] [46]. (A.) The development of cCas-3 and decreased Ki67 were shown with different treatments of 4T1 TNBC tumors in mice. The TDR develops proportionally with cCas-3 [46]. (B.) The release of doxorubicin in the tumor by wHT and mEHT [34].

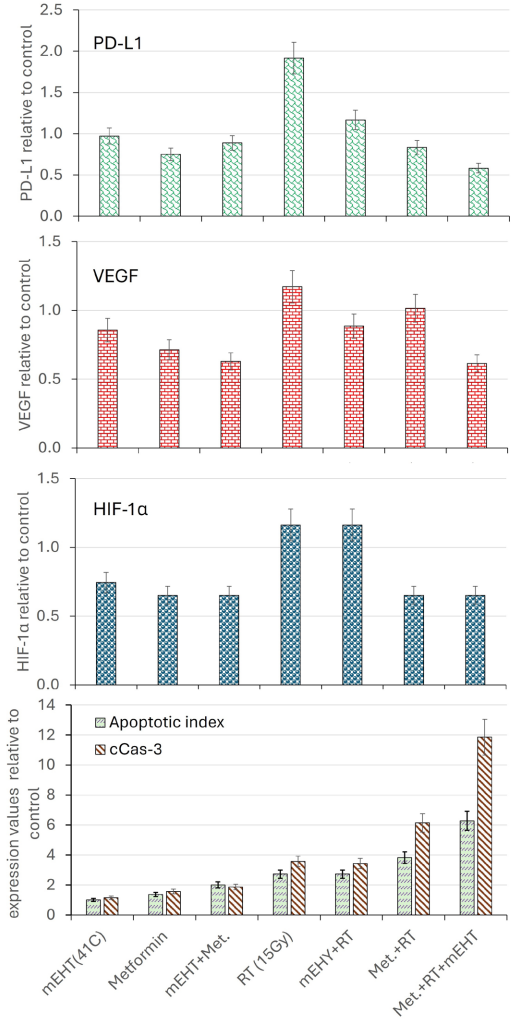

Figure 24. Complementary application of mEHT with Metformin medication. The results are from the 5th day after treatment [31].

Curcumin and resveratrol, effective antioxidants and immune activators were added as medications during the mEHT treatment period of inoculated CT26 cells forming allograft tumors in BALB/c mice. The added medication significantly induced cell cycle arrest and apoptosis of CT26 cells, significantly decreasing the weights of the excised tumors from the euthanized animals [29], Figure 25. The mEHT significantly elevated the serum concentrations of curcumin and resveratrol. The combination induced HSP70 expression while recruiting $CD3^+$ T-cells and $F4/80^+$ macrophages [29].

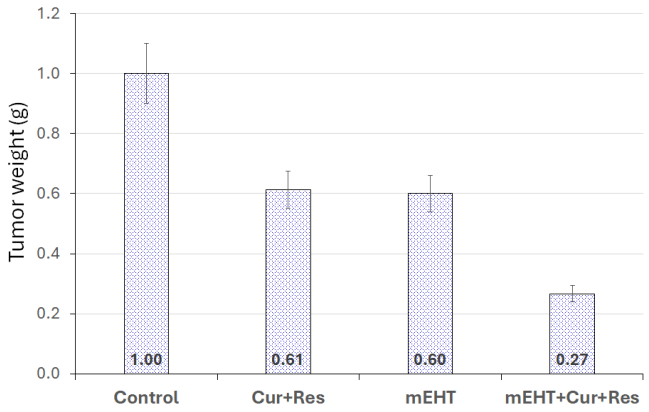

Figure 25. Effect of curcumin and resveratrol on tumor weight excised from the euthanized animals.

Preclinical animal experiments on dogs and cats have a notable advantage because the tumors are naturally developed, not inoculated to the animal. The mEHT treatments of dogs show successful tumor degradation proven by various diagnostic methods, including imaging controls [13]. The treatments of dogs showed significant shrinking of tumors and considerable improvement in the quality of life of the animals [13]. These preclinical treatments, together with the validation of the method, help to optimize the technical solutions of mEHT because the body size of the animal is much larger than that of the rodents, and some of those approach human size, Figure 26. Consequently, these studies can be transferred directly to human clinical applications to develop more precise treatment systems for clinical oncology.

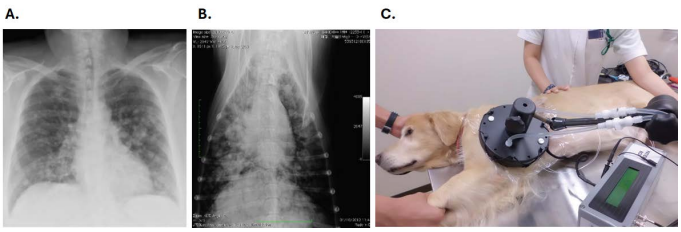

Figure 26. The similarity of the clinical imaging of humans and companion animals. (A.) Pulmonary metastases from recurrent melanoma in a human patient (image courtesy of Dr. DG. Borgeson), (B.) The same lung metastasis of melanoma in a Labrador dog [13]. (C.) mEHT treatment of a dog having pulmonary melanoma metastasis.

Numerous successful veterinary cases were observed [73]. Many cases were treated with mEHT after first or second-line unsuccessful surgery and/or chemotherapy, Figure 27.

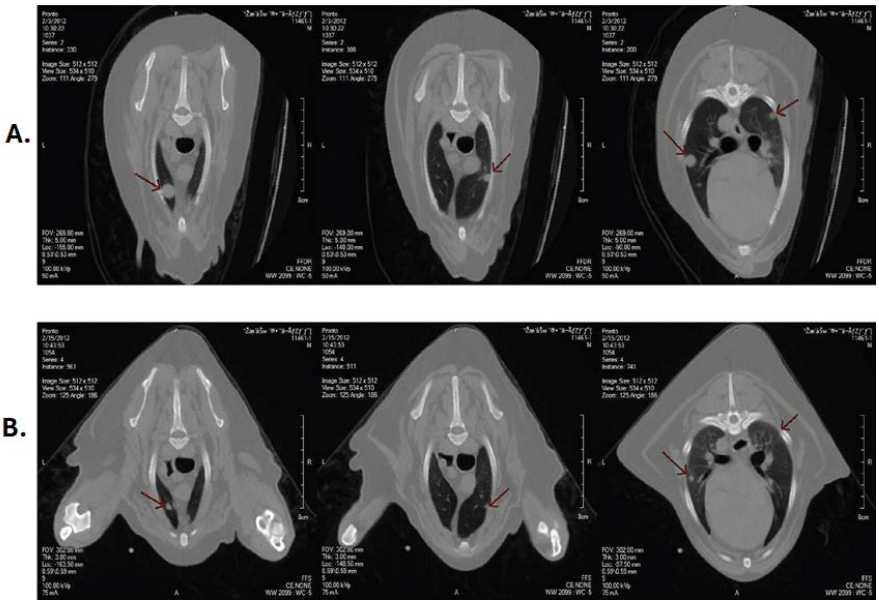

Figure 27. X-ray image of the lung metastasis of melanoma of an 8-year-old male Cocker spaniel. (A.) The images after unsuccessful chemotherapy, before mEHT treatment. The metastatic lesions are pointed by arrows. (B.) The same image after treatment. A significant decrease in the size of the lesions is observed, and some of those completely disappeared.

4. Conclusions

The *in vitro* experiments in the previous part of the series about mEHT results had shown clear pieces of evidence of how the nonthermal electric field, compared to the only thermal treatment (wHT) sinergetically improved the cell destruction [10]. The primary message from the preclinical experiments *in vivo* is that electromagnetic energy absorption has thermal and nonthermal effects appearing synergistically in the mEHT. The strong synergy appears in many comparisons

- The only thermal (iHT) and mEHT treatments declared strong synergy (Figure 9). [40]
- The observed massive appearance of extracellular HSP70 (eHSP70) 72 h post treatment is a strong addition to the thermally developed intracellular iHSP70 induced by hyperthermia (Figure 11).
- The mRNA gene chip results show the characteristic gene up and down regulation differences when the non-thermal effect is active (Figure 12).
- The marked p53 and p21 appear when the non-thermal component is added in Figure 14.
- The effect of modulation in mEHT shows significant changes when the non-thermal addition was given (Figure 17). [37]

- The pulsing treatment (which decreases the thermal but increases the non-thermal absorptions), increases the cell destruction (Figure 18).
- The complementary applications of mEHT with the conventional methods (RT and ChT) also show the advantages of the mEHT.

The well-chosen modulated radiofrequency (RF) signal may trigger resonant excitations of the transmembrane proteins, which triggers extrinsic apoptotic signals. The focused thermal factor generates hyperthermic conditions. The increased temperature provides an appropriate situation for the nonthermal electric field exciting processes by optimizing the chemical reaction rates and enzymatic reactions. The direct thermal and nonthermal effects complete each other, making a complex synergy of mEHT actions, Figure 28.

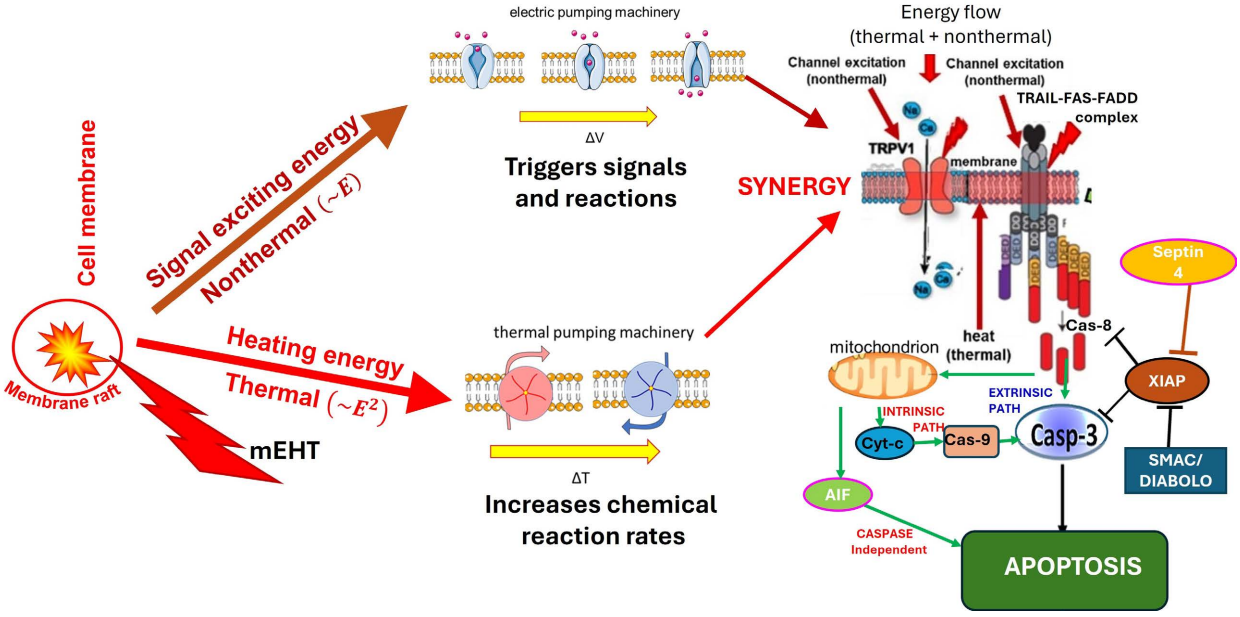

Figure 28. The measured thermal and nonthermal effects of mEHT. The thermal effect has an Arrhenius character, while the nonthermal effects are quantum-mechanical, promoting the enzymatic processes through a transitional state. The thermal conditions optimize and accelerate the nonthermal processes.

The *in vivo* experiments reinforce the previous *in vitro* observations [10], and the physiologic conditions make further support which drives the expectations from the clinical applications. The *in vitro* and *in vivo* proofs verify the usefulness of the mEHT making promises to a significant step forward in human oncology.

Acknowledgements

I am thankful to the listed authors for their diligent research.

Fund

This research received external funding from the Hungarian Government, grant number GINOP_PLUSZ_2.1.1-21-2022-00058.

Conflicts of Interest

The author declares no conflicts of interest regarding the publication of this paper.

References

[1] Escargueil, A. (2023) Feature Reviews in Cancer Therapy. https://www.mdpi.com/journal/cancers/special_issues/reviews_cancer_therapy

[2] Siegel, R.L., Giaquinto, A.N. and Jemal, A. (2024) Cancer Statistics, 2024. *CA*: *A Cancer Journal for Clinicians*, **74**, 12-49. https://doi.org/10.3322/caac.21820

[3] Pancholi, N.J. (2924) Experts Forecast 2024, Part 4: Cutting-Edge Tech for Oncology Drug Discovery, Cancer Research Catalyst. https://www.aacr.org/blog/2024/01/31/experts-forecast-2024-part-4-cutting-edge-tech-for-oncology-drug-discovery/

[4] Szasz, A. (2021) Therapeutic Basis of Electromagnetic Resonances and Signal-Modulation. *Open Journal of Biophysics*, **11**, 314-350. https://doi.org/10.4236/ojbiphy.2021.113011

[5] Szasz, A. (2022) Time-Fractal Modulation—Possible Modulation Effects in Human Therapy. *Open Journal of Biophysics*, **12**, 38-87. https://doi.org/10.4236/ojbiphy.2022.121003

[6] Szasz, A. and Szasz, O. (2020) Time-Fractal Modulation of Modulated Electro-Hyperthermia (MEHT). In: Szasz, A., Ed., Book Challenges and Solutions of Oncological Hyperthermia, Cambridge Scholars, 377-415.

[7] Szasz, O. and Szasz, A. (2016) Nanothermia: A Heterogenic Heating Approach. *Journal of Cancer Research and Therapeutics*, **12**, 1132-1137. https://doi.org/10.4103/0973-1482.197568

[8] Szasz, O. (2019) Bioelectromagnetic Paradigm of Cancer Treatment—Modulated Electro-Hyperthermia (MEHT). *Open Journal of Biophysics*, **9**, 98-109. https://doi.org/10.4236/ojbiphy.2019.92008

[9] Szasz, A. (2022) Heterogeneous Heat Absorption Is Complementary to Radiotherapy. *Cancers*, **14**, Article 901. https://doi.org/10.3390/cancers14040901

[10] Szasz, A. (2024) Preclinical Verification of Modulated Electro-Hyperthermia. Part I. *in Vitro* Research. *International Journal of Clinical Medicine*.

[11] Bini, M., Ignesti, A., Millanta, L., *et al.* (1985) An Unbalanced Electric Applicator for RF Hyperthermia. *IEEE Transactions on Biomedical Engineering*, **32**, 638-641. https://doi.org/10.1109/TBME.1985.325596

[12] Krenacs, T., Meggyeshazi, N., Forika, G., *et al.* (2020) Modulated Electro-Hyperthermia-Induced Tumor Damage Mechanisms Revealed in Cancer Models. *International Journal of Molecular Sciences*, **21**, Article 6270. https://doi.org/10.3390/ijms21176270

[13] Andocs, G., Osaki, T., Tsuka, T., Imagawa, T., *et al.* (2013) Oncothermia Research at Preclinical Level. *Hindawi Publishing Corporation Conference Papers in Medicine*, **2013**, Article ID: 272467. http://Www.Hindawi.Com/Archive/2013/272467/

[14] Szasz, A., Szasz, N. and Szasz, O. (2010) Oncothermia—Principles and Practices. Springer Science. https://link.springer.com/book/10.1007/978-90-481-9498-8

[15] Szasz, A., Szasz, O. and Szasz, N. (2006) Physical Background and Technical Realization of Hyperthermia. In: Baronzio, G.F. and Hager, E.D., Eds., Hyperthermia in Cancer Treatment: A Primer, Springer, 27-59.

https://doi.org/10.1007/978-0-387-33441-7_3

[16] Szasz, A. (2015) Bioelectromagnetic Paradigm of Cancer Treatment Oncothermia. In: Rosch, P.J., Ed., Bioelectromagnetic and Subtle Energy Medicine, CRC Press and Taylor & Francis Group, 323-336.

[17] Szasz, A. (2014) Oncothermia: Complex Therapy by EM and Fractal Physiology. 2014 *XXXIth URSI General Assembly and Scientific Symposium*, Beijing, 16-23 August 2014.

[18] Kim, W., Kim, M.S., Kim, H.J., *et al.* (2017) Role of HIF-1*α* in Response of Tumors to a Combination of Hyperthermia and Radiation *in vivo*. *International Journal of Hyperthermia*, **34**, 276-283. https://doi.org/10.1080/02656736.2017.1335440

[19] Portoro, I., Danics, L. and Veres, D. (2018) Increased Efficacy in Treatment of Glioma by a New Modulated Electro-Hyperthermia (MEHT) Protocol. *Oncothermia Journal*, **24**, 344-356.

[20] Danics, L., Schvarcz, C.S., Viana, P., *et al.* (2020) Exhaustion of Protective Heat Shock Response Induces Significant Tumor Damage by Apoptosis after Modulated Electro-Hyperthermia Treatment of Triple Negative Breast Cancer Isografts in Mice. *Cancers*, **12**, Article 2581. https://pubmed.ncbi.nlm.nih.gov/32927720/

[21] Jeon, T.-W., Yang, H., Lee, C.G., O, S.T., *et al.* (2016) Electro-Hyperthermia Up-Regulates Tumour Suppressor Septin 4 to Induce Apoptotic Cell Death in Hepatocellular Carcinoma. *International Journal of Hypertension*, **7**, 1-9. https://doi.org/10.1080/02656736.2016.1186290

[22] Cha, J., Jeon, T.-W., Lee, C.-G., *et al.* (2015) Electro-Hyperthermia Inhibits Glioma Tumorigenicity Through the Induction of E2F1-Mediated Apoptosis. *International Journal of Hyperthermia*, **31**, 784-792. https://doi.org/10.3109/02656736.2015.1069411

[23] Meggyeshazi, N., Andocs, G., Balogh, L., *et al.* (2014) DNA Fragmentation and Caspase-Independent Programmed Cell Death by Modulated Electrohyperthermia. *Strahlentherapie und Onkologie*, **190**, 815-822. https://doi.org/10.1007/s00066-014-0617-1

[24] Andocs, G., Meggyeshazi, N., Balogh, L., *et al.* (2014) Upregulation of Heat Shock Proteins and the Promotion of Damage-Associated Molecular Pattern Signals in a Colorectal Cancer Model by Modulated Electrohyperthermia. *Cell Stress and Chaperones*, **20**, 37-46. https://doi.org/10.1007/s12192-014-0523-6

[25] Meggyeshazi, N., Andocs, G. and Krenacs, T. (2013) Programmed Cell Death Induced by Modulated Electro-Hyperthermia. *Hindawi Publishing Corporation Conference Papers in Medicine*, **2013**, Article ID: 187835.

[26] Vancsik, T., Kovago, C.S., Kiss, E., *et al.* (2018) Modulated Electro-Hyperthermia Induced Loco-Regional and Systemic Tumor Destruction in Colorectal Cancer Allografts. *Journal of Cancer*, **9**, 41-53. https://doi.org/10.7150/jca.21520

[27] Tsang, Y.-W., Huang, C.-C., Yang, K.-L., *et al.* (2015) Improving Immunological Tumor Microenvironment Using Electro-Hyperthermia Followed by Dendritic Cell Immunotherapy. *BMC Cancer*, **15**, Article 708. http://Www.Ncbi.Nlm.Nih.Gov/Pubmed/26472466

[28] Vancsik, T., Mathe, D., Horvath, I., *et al.* (2021) Modulated Electro-Hyperthermia Facilitates NK-Cell Infiltration and Growth Arrest of Human A2058 Melanoma in a Xenograft Model. *Frontiers in Oncology*, **11**, Article 590764. https://www.frontiersin.org/articles/10.3389/fonc.2021.590764/full

[29] Kuo, I.-M., Lee, J.-J., Wang, Y.-S., *et al.* (2020) Potential Enhancement of Host

Immunity and Anti-Tumor Efficacy of Nanoscale Curcumin and Resveratrol in Colorectal Cancers by Modulated Electro-Hyperthermia. *BMC Cancer*, **20**, Article 603. https://pubmed.ncbi.nlm.nih.gov/32600429/

[30] Besztercei, B., Vancsik, T., Benedek, A., *et al.* (2019) Stress-Induced, P53-Mediated Tumor Growth Inhibition of Melanoma by Modulated Electrohyperthermia in Mouse Models Without Major Immunogenic Effects. *International Journal of Molecular Sciences*, **20**, Article 4019. https://Www.Mdpi.Com/1422-0067/20/16/4019

[31] Kim, H., Kim, D., Kim, W., *et al.* (2022) The Efficacy of Radiation Is Enhanced by Metformin and Hyperthermia Alone or Combined against FSaII Fibrosarcoma in C3H Mice. *Radiation Research*, **198**, 190-199. https://doi.org/10.1667/RADE-21-00231.1

[32] Prasad, B., Kim, S., Cho, W., *et al.* (2019) Quantitative Estimation of the Equivalent Radiation Dose Escalation Using Radiofrequency Hyperthermia in Mouse Xenograft Models of Human Lung Cancer. *Nature*, **9**, Article 3942. https://www.nature.com/articles/s41598-019-40595-6

[33] Kim, J.-K., Prasad, B. and Kim, S. (2017) Temperature Mapping and Thermal Dose Calculation in Combined Radiation Therapy and 13.56 MHz Radiofrequency Hyperthermia for Tumor Treatment. *Optical Methods for Tumor Treatment and Detection: Mechanisms and Techniques in Photodynamic Therapy XXVI*, San Francisco, 28-29 January 2017, Article ID: 1004718. http://spie.org/publications/proceedings/paper/10.1117/12.2253163?origin_id=x4318

[34] Tsang, Y.-W., Chi, K.-H., Huang, C.-C., Chi, M.-S., *et al.* (2019) Modulated Electro-Hyperthermia-Enhanced Liposomal Drug Uptake by Cancer Cells. *International Journal of Nanomedicine*, **14**, 1269-1579. https://doi.org/10.2147/IJN.S188791

[35] Balogh, L., Polyak, A., Postenyi, Z., *et al.* (2016) Temperature Increase Induced by Modulated Electrohyperthermia (Oncothermia®) in the Anesthetized Pig Liver. *Journal of Cancer Research and Therapeutics*, **12**, 1153-1159. https://doi.org/10.4103/0973-1482.197561

[36] Kovago, C.S., Meggyeshazi, N., Andocs, G. and Szasz, A. (2013) Report of the Pilot-Study Done for the Proposed Investigation on the Possible Synergic Effect Between High Dose Ascorbic Acid Application and Oncothermia Treatment. *Hindawi Publishing Corporation Conference Papers in Medicine*, **2013**, Article ID: 386913.

[37] Wust, P., Veltsista, P.D., Oberacker, E., Yavvari, P., Walther, W., Bengtsson, O., *et al.* (2022) Radiofrequency Electromagnetic Fields Cause Non-Temperature-Induced Physical and Biological Effects in Cancer Cells. *Cancers*, **14**, Article 5349. https://Www.Mdpi.Com/2072-6694/14/21/5349

[38] Meggyeshazi, N., Andocs, G., Spisak, S., *et al.* (2013) Early Changes in MRNA and Protein Expression Related to Cancer Treatment by Modulated Electro-Hyperthermia. *Hindawi Publishing Corporation Conference Papers in Medicine*, **2013**, Article ID: 249563.

[39] Prasad, B., Kim, S., Cho, W., *et al.* (2018) Effect of Tumor Properties on Energy Absorption, Temperature Mapping, and Thermal Dose in 13,56-MHz Radiofrequency Hyperthermia. *Journal of Thermal Biology*, **74**, 281-289. https://doi.org/10.1016/j.jtherbio.2018.04.007

[40] Andocs, G., Renner, H., Balogh, L., Fonyad, L., Jakab, C. and Szasz, A. (2009) Strong Synergy of Heat and Modulated Electro—Magnetic Field in Tumor Cell Killing, Study of HT29 Xenograft Tumors in a Nude Mice Model. *Strahlentherapie Und Onkologie*, **185**, 120-126. https://doi.org/10.1007/s00066-009-1903-1

[41] Danics, L., Schvarcz, C.S. and Zolcsak, Z. (2018) Modulated Electro Hyperthermia Inhibits Tumor Progression in a Triple Negative Mouse Breast Cancer Model. *Oncothermia Journal*, **24**, 442-454.

[42] Thomas, M.B., Major, E., Benedek, A., Horváth, I., Máthé, D., Bergmann, R., *et al.* (2020) Suppression of Metastatic Melanoma Growth in Lung by Modulated Electro-Hyperthermia Monitored by a Minimally Invasive Heat Stress Testing Approach in Mice. *Cancers*, **12**, Article 3872. Https://Pubmed.Ncbi.Nlm.Nih.Gov/33371498/

[43] Schvarcz, C.S.A., Danics, L., Krenacs, T., Viana, P., Beres, R., *et al.* (2021) Modulated Electro-Hyperthermia Induces a Prominent Local Stress Response and Growth Inhibition in Mouse Breast Cancer Isografts. *Cancers*, **13**, Article 1744. https://Pubmed.Ncbi.Nlm.Nih.Gov/33917524/

[44] Matsumoto, Y., Hayshi, J., Sekino, Y., Fukumitsu, N., Saito, T., Ishikawa, H. and Sakurai, H. (2018) Radio-Sensitization Effect of Novel Cancer Therapy, Oncothermia ~ Toward Overcoming Treatment Resistance. 2018 *Annual Conference of Japanese Hyperthermia Society*, Fukui, 26-28 March 2018.

[45] Qin, W., Akutsu, Y., Andocs, G., *et al.* (2014) Modulated Electro-Hyperthermia Enhances Dendritic Cell Therapy Through an Abscopal Effect in Mice. *Oncology Reports*, **32**, 2373-2379. https://doi.org/10.3892/or.2014.3500

[46] Aloss, K., Bokhari, S.M.Z., Leroy Viana, P.H., Giunashvili, N., Schvarcz, C.A., SzénáSi, G., *et al.* (2024) Modulated Electro-Hyperthermia Accelerates Tumor Delivery and Improves Anticancer Activity of Doxorubicin Encapsulated in Lyso-Thermosensitive Liposomes in 4T1-Tumor-Bearing Mice. *International Journal of Molecular Sciences*, **25**, Article 3101. https://doi.org/10.3390/ijms25063101

[47] Son, B., Jeon, J., Lee, S., *et al.* (2019) Radiotherapy in Combination with Hyperthermia Suppresses Lung Cancer Progression via Increased NR4A3 and KLF11 Expression. *International Journal of Radiation Biology*, **95**, 1696-1707. https://doi.org/10.1080/09553002.2019.1665213

[48] Yang, W., Gwan, H.H., Shin, H.-Y., *et al.* (2018) Combined Treatment with Modulated Electro-Hyperthermia and an Autophagy Inhibitor Effectively Inhibit Ovarian and Cervical Cancer Growth. *International Journal of Hyperthermia*, **36**, 9-20. https://doi.org/10.1080/02656736.2018.1528390

[49] Andocs, G., Okamoto, Y., Kawamotot., Osaki, T., Tsuka, T., Imagawa, T., Minami, S., Balogh, L., Meggyeshazi, N. and Szasz, O. (2013) Oncothermia Basic Research at *in Vivo* Level. The First Results in Japan. *Hindawi Publishing Corporation Conference Papers in Medicine*, **2013**, Article ID: 197328.

[50] Szasz, O. (2011) Temperature Measurements during Oncothermia (Collection of Temperature Measurements in Loco Regional Hyperthermia). *Oncothermia Journal*, **4**, 62-86.

[51] Lee, S.-Y., Kim, J.-H., Han, Y.-H., *et al.* (2018) The Effect of Modulated Electro-Hyperthermia on Temperature and Blood Flow in Human Cervical Carcinoma. *International Journal of Hyperthermia*, **34**, 953-960. https://doi.org/10.1080/02656736.2018.1423709

[52] Meggyeshazi, N. (2015) Studies on Modulated Electrohyperthermia Induced Tumor Cell Death in a Colorectal Carcinoma Model. Ph.D Thesis, Semmelweis University. https://www.google.com/url?sa=t&source=web&rct=j&opi=89978449&url=https://repo.lib.semmelweis.hu/bitstream/handle/123456789/3956/meggyeshazinora.e.pdf%3Fsequence%3D4&ved=2ahUKEwiesKr1p8KHAxWoHhAIHQVICa0QFnoECBIQ

AQ&usg=AOvVaw3tij1E3KOP_pDGIjoDDGLI

[53] Andocs, G., Rehman, M.U., Zhao, Q.-L., Tabuchi, Y., Kanamori, M. and Kondo, T. (2016) Comparison of Biological Effects of Modulated Electro-Hyperthermia and Conventional Heat Treatment in Human Lymphoma U937 Cell. *Cell Death Discovery* (*Nature Publishing Group*), **2**, Article 16039. https://www.nature.com/articles/cddiscovery201639

[54] Andocs, G. (2010) Revealing the Mechanism of Action of Modulated Electrothermia Experimentally in Animal Model (HT29 Colorectal Xenograft Study). *Annual Meeting of Society for Thermal Medicine*, Florida, 23-26 April, 2010.

[55] Szasz, A. (2022) Time-Fractal in Living Objects. *Open Journal of Biophysics*, **12**, 1-26. https://doi.org/10.4236/ojbiphy.2022.121001

[56] de Loof, M., de Jong, S. and Kruyt, F.A.E. (2019) Multiple Interactions Between Cancer Cells and the Tumor Microenvironment Modulate TRAIL Signaling: Implications for TRAIL Receptor Targeted Therapy. *Frontiers in Immunology*, **10**, Article 1530. https://doi.org/10.3389/fimmu.2019.01530

[57] de Andrade Mello, P., Bian, S., Savio, L.E.B., *et al.* (2017) Hyperthermia and Associated Changes in Membrane Fluidity Potentiate P2X7 Activation to Promote Tumor Cell Death. *Oncotarget*, **8**, 67254-67268. https://doi.org/10.18632/oncotarget.18595

[58] Meggyeshazi, N., Andocs, G., Spisak, S., *et al.* (2013) Modulated Electrohyperthermia Causes Caspase Independent Programmed Cell Death in HT29 Colon Cancer Xenografts. *Virchows Archiv*, **463**, Article 329.

[59] Meggyeshazi, N., Andocs, G., Balogh, L. and Krenacs, T. (2011) DNA Fragmentation-Driven Tumor Cell Degradation Induced by Modulated Electro-Hyperthermia. *Virchows Archiv*, **459**, S204-S205.

[60] Yang, K.-L., Huang, C.-C., Chi, M.-S., Chiang, H.-C., Wang, Y.-S., Andocs, G., *et al.* (2016) *In Vitro* Comparison of Conventional Hyperthermia and Modulated Electro-Hyperthermia. *Oncotarget*, **7**, 84082-84092. Http://Www.Ncbi.Nlm.Nih.Gov/Pubmed/27556507

[61] Springer, M. and Paulsson, J (2006) Harmonies From Noise. *Nature*, **439**, 27-28. https://doi.org/10.1038/439027a

[62] West, J.B. (2013) Fractal Physiology and Chaos in Medicine. World Scientific. https://doi.org/10.1142/8577

[63] Astumian, R.D. and Chock, P.B. (1989) Effects of Oscillations and Energy-Driven Fluctuations on the Dynamics of Enzyme Catalysis and Free-Energy Transduction. *Physical Review A*, **39**, 6416-6435. https://doi.org/10.1103/PhysRevA.39.6416

[64] O'Neill, D.P., Peng, T., Stiegler, P., Mayrhauser, U., Koestenbauer, S., Tscheliessnigg, K., *et al.* (2011) A Three-State Mathematical Model of Hyperthermic Cell Death. *Annals of Biomedical Engineering*, **39**, 570-579. https://doi.org/10.1007/s10439-010-0177-1

[65] Kiss, E., Andocs, G., Meggyeshazi, N., Vancsik, T., Kovago, C.S., Papp, E. and Krenacs, T. (2015) The Role of Modulation in Modulated Electro-Hyperthermia (MEHT). 36*th Conference of International Clinical Hyperthermia Society* (ICHS), Bad Salzhausen, July 10 2015. https://doi.org/10.1016/j.eujim.2016.08.087

[66] Szasz, O., Andocs, G. and Meggyeshazi, N. (2013) Modulation Effect in Oncothermia. *Hindawi Publishing Corporation Conference Papers in Medicine*, **2013**, Article ID: 395678.

[67] Forika, G., Balogh, A., Vancsik, T., Zalatnai, A., *et al.* (2020) Modulated Elec-

tro-Hyperthermia Resolves Radioresistance of Panc1 Pancreas Adenocarcinoma and Promotes DNA Damage and Apoptosis *in Vitro*. *International Journal of Molecular Sciences*, **21**, Article 5100. https://doi.org/10.3390/ijms21145100

[68] Andocs, G., Okamoto, Y., Kawamotot, K., Osaki, T., Tsuka, T., Imagawa, T., Minami, S., Balogh, L., Meggyeshazi, N. and Szasz, O. (2013) Oncothermia Basic Research at *in vivo* Level. The First Results in Japan. *Oncothermia Journal*, **7**, 296-300. https://doi.org/10.1155/2013/197328

[69] Plotnikov, A., Fishman, D., Tichler, T., Korenstein, R. and Keisari, Y. (2004) Low Electric Field Enhanced Chemotherapy Can Cure Mice with CT-26 Colon Carcinoma and Induce Anti-Tumor Immunity. *Clinical and Experimental Immunology*, **138**, 410-416. https://doi.org/10.1111/j.1365-2249.2004.02636.x

[70] Kirson, E.D., Schneiderman, R.S., Dbaly, V., *et al*. (2009) Chemotherapeutic Treatment Efficacy and Sensitivity Are Increased by Adjuvant Alternating Electric Fields (TTFields). *BMC Medical Physics*, **9**, Article No. 1. https://doi.org/10.1186/1756-6649-9-1

[71] Schneiderman, R.S., Shmueli, E., Kirson, E.D. and Palti, Y. (2010) TTFields Alone and in Combination with Chemotherapeutic Agents Effectively Reduce the Viability of MDR Cell Sub-Lines that Over-Express ABC Transporters. *BMC Cancer*, **10**, Article 229. https://doi.org/10.1186/1471-2407-10-229

[72] Needham, D., Anyarambhatla, G., Kong, G. and Dewhirst, M.W. (2000) A New Temperature-Sensitive Liposome for Use with Mild Hyperthermia: Characterization and Testing in a Human Tumor Xenograft Model. *Cancer Research*, **60**, 1197-201.

[73] Balogh, L., Andocs, G., Thuroczy, J., Polyak, A., Szasz, O. and Szasz, A. (2009) Oncological and Non-Oncological Applications of Electromagnetic Hyperthermia (Oncothermia) in the Veterinary Clinics—2 Years of Experience. *Poster Presentation at* 1 *International es Oncothermie-Symposium*, Köln, 22-23 November 2009.

Abbreviations

CDK	cyclin-dependent kinase
ChT	chemotherapy
DAMP	damage associated molecular pattern
DC	dendritic cell
DNA	deoxyribonucleic acid
HMGB1	high-mobility group protein
HSP	heat-shock protein
ICD	immunogenic cell death
mEHT	modulated electro-hyperthermia
NK cell	natural killer cell
PCR	polymerase chain reaction
ROS	reactive oxygen species
RT	radiotherapy
Op	surgery
TDR	tumor destruction ratio
TRAIL	tumour-necrosis factor related apoptosis inducing ligand
XIAP X-	linked Inhibitor of apoptosis